This Project has received funding from European Commission by means of Horizon 2020,
the EU Framework Programme for Research and Innovation, under Grant Agreement no.727348

Grant Agreement No. 727348

Project Acronym:

SOCRATCES

Project title:

SOlar Calcium-looping integRAtion for Thermo-Chemical Energy Storage.

DELIVERABLE D3.4

Solar Calciner Design

Funding scheme:	Research and Innovation Action (RIA)		
Project Coordinator:	USE		
Start date of the project:	01.01.2018	**Duration of the project:**	36 months
Contractual delivery date:	Month 12		
Actual delivery date:	28.12.2018		
Contributing WP:	WP3		
Dissemination level:	*Public*		
Authors:	Tom Hills (Calix) Pilar Lisbona (Universidad de Zaragoza)		
Contributors:	Simon Thomsen (Calix) Luis Romeo (Universidad de Zaragoza) Mark Sceats (Calix) Carlos Ortiz (Universidad de Sevilla)		
Version:	V2		
Document name	**SOCRATCES_D3.4_final**		

SUMMARY

This deliverable explains the evolution of calciner design since the beginning of the SOCRATCES project. Several major alterations have taken place due to thermodynamic, kinetic and energetic constraints. This deliverable solely relates to the design of the Calciner for the SOCRATCES pilot plant at laboratory scale, while taking into account the implications for a large scale pilot plant where appropriate.

The primary outcomes from the reported activities are to adopt a Calciner design in which:-

1. The process temperature is > 900°C at about 1 bar CO_2; and
2. Includes an auxiliary electrical heating system for control, start-up and testing; and
3. Coupling to the solar field is accomplished by an indirect irradiation so the reactor is an annular design which surrounds the cavity solar receiver.

The deliverable is split in to three sections. The first explains the change in thinking around the optimal overall process flow for the calciner side of SOCRATCES, based on thermodynamics and kinetics. Part Two looks at the of the solar calciner design proposals and analyses the chosen design. Part Three explains the modelling of the calciner.

The plan to calcine at temperatures below 700 °C has been abandoned for two main reasons. Firstly, the low temperature means that only a slow rate of calcination was possible, even with

relatively large thermodynamic driving forces. Secondly, calcination conditions at 700 °C are achieved only below 3% CO_2 at 1 atm; large amounts of diluent would be required to produce even the smallest thermodynamic driving force. This would require either large membrane separation systems which would consume most of the primary energy generated by the solar field, or the raising of large volumes of steam, with the inefficiencies inherent in that and in heating the steam to the desired temperature.

As a consequence, the calcination temperature was changed to >900 °C to enable calcination in pure CO_2 and thus elimination of gas separation requirements. It also enables relatively fast kinetics at, say, 920 °C despite a pure CO_2 atmosphere.

Several reactor designs were developed. These are explained below, with their benefits and disadvantages. Eventually, a design with a cavity solar receiver surrounded by a reaction annulus was chosen. Simulations and calculations of the design have informed more detailed solar calciner design. The chosen design includes:

1. a cavity solar receiver surrounded by a reaction annulus chosen to minimise radiation and heat losses; and
2. an auxiliary electric heating system that allows for trimming of the operation of the reactor to deliver fixed dispatchable power, independent of the solar power variations, and for testing the design.

Approximate sizes and operational methods have been developed, which will be refined during WP6 with continuing input from WP3's simulations.

In Part 3, the solar-electric calciner design was checked using models of the process. Virtually full calcination was found to occur under conditions where the flux through the reactor wall was controlled by auxiliary power.

TABLE OF CONTENTS

PART ONE: CONCEPT SCOPING

1. INTRODUCTION AND INITIAL PROBLEM STATEMENT

SOCRATCES aims to reduce the cost of storing solar energy and generating dispatchable power on demand by using calcium looping to convert the solar energy to chemical energy in the form of reactive calcium oxide (CaO) via calcination of limestone ($CaCO_3$). The calcium oxide is carbonated using CO_2, releasing around 3180 kJ/kg CaO for power generation as it returns to $CaCO_3$. This cycle has not been performed on the proposed scale before.

The storage requirement of SOCRATCES is such that the efficient storage of thermal energy from carbonation over the diurnal timescales is limited by heat losses during storage and subject to seasonal variations, so that the design is based on (a) a requirement to heat the limestone from ambient temperature as a worst case (which is required for start-up and testing) and (b) the fact that the calcination and carbonation would not occur at the same time and the heat losses from the variable storage time are subject to latitude variations during the year [1]. The two processes of calcination and carbonation are married together by the storage of CO_2 and CaO ready for recombination when energy is required.

Work Package 3 concentrates on the calciner side of the cycle. The calciner has one main objective – to calcine limestone using concentrated solar power. The SOCRATCES proposal provides advice on how this can be achieved:

- The calciner must operate at temperatures of less than 700 °C to allow use of conventional concentrated solar power technology and thermal coupling to the carbonator;
- Calcination should take place in helium or steam, with CO_2;

The initial problem statement can be written as a question:

How can we best achieve efficient and controlled calcination of limestone using solar energy at temperatures less than 700 °C in atmospheres of helium and/or steam?

From the work carried out for this deliverable, the updated problem statement is desirably less restrictive, namely:

How can we best achieve efficient and controlled calcination of limestone using solar energy?

The rest of the deliverable is set out as follows:

- Discussion of the thermodynamic and kinetic constraints of the process;
- Proposed designs for the calciner system;
- Analysis of the chosen design
- Future work and way forward.

2. FLASH CALCINERS

Calix has developed and patented a flash calciner design which is used commercially to make very high surface area magnesium oxide from magnesium carbonate. Many other minerals can be used as feedstock, and in the LEILAC project a large-scale natural gas-fired Calix Flash Calciner (CFC) is being built to calcine limestone and cement raw meal for the lime and cement industries as a replacement to the calciner and pre-calciner in those industries [2]. While LEILAC is focussing on scale-up to large pilot scale whilst using the same fuel, natural gas, as is used in Calix's current CFCs, SOCRATCES focusses on a fundamental redesign of the CFC to accommodate the use of concentrated solar radiation.

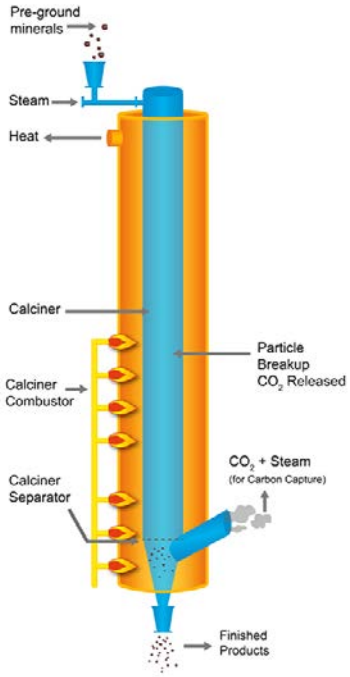

Figure 1: A co-current Calix Flash Calciner (CFC) fired by natural gas [3]

A CFC is, at its most simple, a heated tube. Ground mineral particles are passed down the tube and are irradiated by the hot walls of the reactor tube. This heats them up and leads to thermal decomposition, releasing a gas. The process is extremely fast for materials ground to a powder less than about 50 microns, taking only a few tens of seconds for the particles to be heated by hundreds of degrees, decomposed and then cooled. This very fast decomposition (or 'flash calcination') produces powder materials with exceptionally high surface areas and unique surface properties due to the high density of edges and corners on the particles and their pores which have similar properties to nanomaterials. As a consequence, these micron-sized particles are said to be 'nano-active' [3].

Figure 1 shows a simple diagram of a CFC, fired by natural gas and processing finely ground carbonate minerals to an oxide. As shown, steam can be introduced to fluidise the particles, and improve heat transfer. The design of the reactor of Figure 1 is based on the steam being about 0-10% v/v of the gas at the exhaust. An important feature of the CFC is that the combustion gases do not come in to contact with the reactor gases. This means that any gases that emanate from the reaction are produced pure, or, when steam is added, are an easily separable mix of reaction gas and steam. In the case of carbonate minerals, a pure stream of CO_2 is formed which, after de-dusting, is suitable for compression and export to carbon capture and storage (CCS) transport and storage infrastructure. The elimination of expensive capture processes which concentrate the CO_2 from a flue gas at 3–30% CO_2 to >95% CO_2, means that CFCs promise to reduce the cost of capture of such process CO_2 in several important industries such as cement manufacture and lime production at dedicated sites, but also in diverse industries such as steel mills and Kraft mills.

2.1. The terminal velocity of particles in CFCs

The fast rate of reaction is key for the success of CFCs for two main reasons. First of all, it produces a more reactive, and thus valuable, product. Secondly, it reduces the size of the reactor. The residence time of the powder is simply the time it takes to fall from the top to the bottom of the CFC, and so shortening a reactor will, for an otherwise identical set-up, reduce the residence time.

The terminal velocity (i.e. maximum speed of falling) of a particle is dictated by Stokes' Law [4]:

$$v_{p0} = \frac{2(\rho_p - \rho_f)a^2 g}{9\mu}$$

Here, v_{p0} is the terminal velocity, ρ_p is the density of the particles (kg/m^3), ρ_f is the density of the gas (kg/m^3), a^2 is the particle's surface area of the maximum cross-section perpendicular to the direction of fall of the particle (m^2), g is gravitational acceleration (m/s^2) and μ is the dynamic viscosity of the fluid (Pa.s). From this equation it can be determined that in more dense, viscous fluids a particle will fall less quickly. As gases heat up, they become both slightly more viscous but significantly less dense. This leads to the conclusion that the ratio of $(\rho_p - \rho_f)/\mu$ dictates the relationship between temperature and terminal velocity. Stokes' Law is applied to a particle in CO_2 in Figure 2, showing the terminal velocity falls with temperature. Despite the fluid density at 800 °C falling to a quarter that at 0 °C, the difference between the particle and fluid density changes very little – by less than 0.1%. Over that period, the viscosity more than triples.

Thermal decomposition leads to the emission of gas and thus mass. There is often a modest change in volume, too, but the calcined product often has a lower density than limestone, of perhaps 1300 kg/m^3 rather than 1900 kg/m^3. This will reduce the terminal velocity by around a third upon full calcination.

Stokes' Law applies to particles falling through stagnant gas. If the gas has vertical flow, the actual velocity of the particle relative to a stationary object (say, a reactor wall) is different. A CFC can exploit this phenomenon. If gases flow 'co-current' (downwards) with the particles, the particles will fall faster and if the gases flow 'counter-current' (upwards) to the particles, the particles will fall slower and their residence time will increase.

Other important phenomena are that particles may be injected as agglomerates from attractive forces, or may form streamers to minimise the gas-particle friction. These increase the effective hydrodynamic diameter of the particles, and will be discussed later [4].

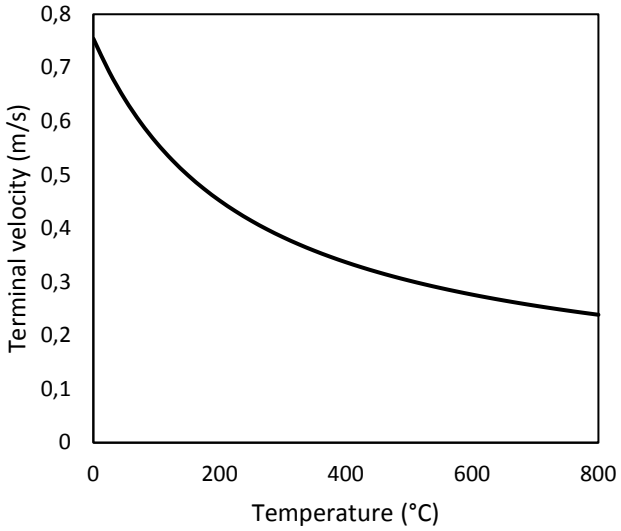

Figure 2: Effect of temperature on terminal velocity of a 50 µm, 1900 kg/m^3 particle in 1 atm CO_2 according to Stokes' Law [5]

3. THE THERMODYNAMICS AND KINETICS OF CALCINATION

Calcination is the thermal decomposition of a carbonate mineral. In this case, the mineral is limestone (calcium carbonate, $CaCO_3$), which decomposes to lime (calcium oxide, CaO) and carbon dioxide (CO_2):

$$CaCO_{3\,(s)} \leftrightarrow CaO_{(s)} + CO_{2\,(g)}$$

The reaction is endothermic, needed around 178 kJ/mol [6]. It is reversible; the recombination of CaO and CO_2 is called carbonation, and it releases 178 kJ/mol when it occurs.

The direction of reaction is dependent upon temperature and the partial pressure of CO_2 (as well, to a small extent, upon the morphology of the $CaCO_3$). In general, at low partial pressures and high temperatures calcination occurs, and at high partial pressures and low temperatures carbonation occurs. On a graph with an x-axis of temperature and a y-axis of partial pressure the two directions of reaction occupy adjacent regions: calcination is in the bottom-right and carbonation in the top-left. The line which separates them is known as the equilibrium curve. It is often calculated as a partial pressure which is a function of temperature. An accepted definition of the equilibrium curve is

$$p^*_{CO_2} = 4.137 \times 10^9 e^{\frac{-20474}{T}}$$

Here, p^*_{CO2} is the equilibrium partial pressure of CO_2 in kPa for the decomposition of calcium carbonate and T is the absolute temperature in K [7]. This temperature dependence is shown in Figure 3. Values are shown in Table 1, too. To effect calcination it is necessary for the actual partial pressure of CO_2 to be lower than the equilibrium partial pressure. For example, at 700 °C the partial pressure of CO_2 surrounding the calcium carbonate must be lower than 0.0301 bara.

Table 1: Equilibrium partial pressure of CO_2 for the thermal composition (calcination) of calcium carbonate, 650–950 °C

Temperature (°C)	Equilibrium partial pressure, bara
650	0.0096
700	0.0301
750	0.0841
800	0.2137
850	0.4997
900	1.0870
950	2.2190

It is important to note that the equilibrium pressure is a partial pressure, not a total pressure. Taking again the example at 700 °C, if the total pressure was lower than 0.0301 bara then limestone would still calcine in a pure CO_2 atmosphere. At atmospheric pressure (1.013 bara), the molar fraction of CO_2 must be less than (0.0301*1.013 =) 3.05%. Equally, at 10 atm the CO_2 molar fraction could only be 0.305%.

During discussions with WP6 it became clear that designing a vacuum calciner at the proposed pilot scale would be unacceptable from a technical, time, safety and cost point-of-view (and would be uneconomical at demonstrator scale). Thus, it is assumed throughout the rest of the deliverable that the calciner operates at atmospheric pressure, i.e. 1.013 bara = 1 atm. Given this constraint, the atmosphere in a calciner at 700 °C can be a maximum of 3.05% CO_2 if calcination is to occur and recarbonation is to be avoided. To achieve this, there must be 32

moles of other 'diluent' gases for every mole of CO_2 in the calciner. Continuous calcination implies continuous generation of CO_2, which will increase the partial pressure of CO_2. Thus, the gas in the reactor must be removed and replaced with a diluent gas to achieve the required low CO_2 partial pressure.

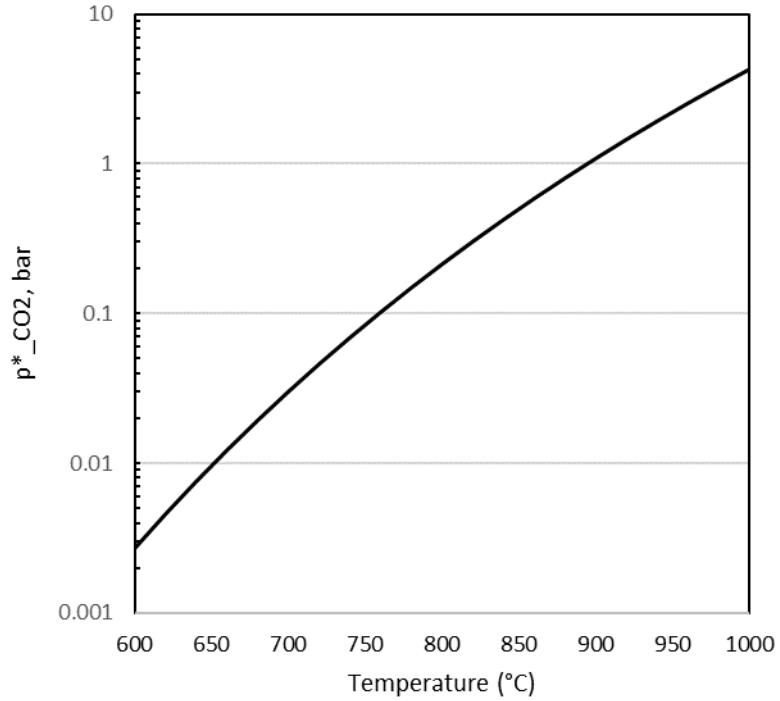

Figure 3: The temperature dependence of the equilibrium partial pressure of CO_2 of the thermal decomposition of calcium carbonate [7]

3.1. Calcination in helium

SOCRATCES proposes two diluent gases – helium and steam. Helium's benefits are that it is beneficial for convective heat transfer and as a small molecule it can be easily separated from the much larger CO_2 by membranes. Steam's benefits are that it is easy to generate and very easy to separate from CO_2 by condensation.

Figure 4 shows a simple example of the helium process. Calcium carbonate and helium enter the calciner. A stream of CaO exhausts the calciner for storage. The helium and CO_2 generated by calcination exhaust the calciner as a gas stream which enters a gas separation unit. Here, they are separated and the CO_2 is stored whilst the helium enters a small storage unit ready for reinjection in to the calciner. Note that some intermediate stages (de-dusting of the gas stream, cooling of the CaO stream) have been omitted for clarity.

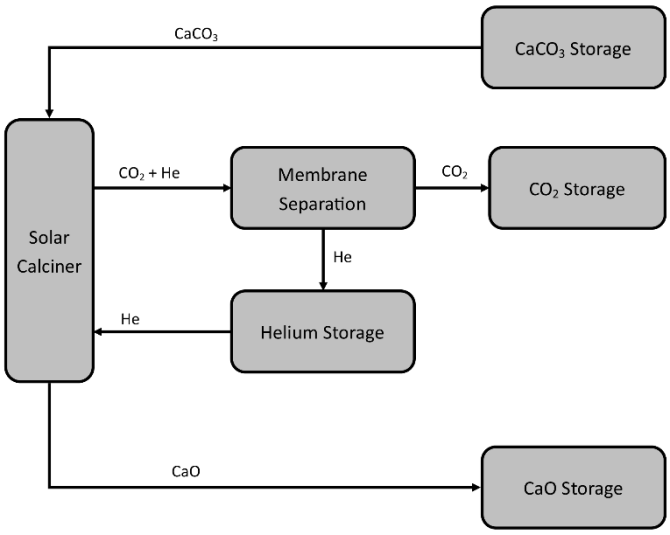

Figure 4: Solar calcination using helium as a diluent

3.1.1. Compression Costs

The most important unit of this process, excluding the solar calciner, is the gas separation unit. Membrane separation units are an option, and work because some molecules are more capable of passing a semi-permeable membrane. This means that, in this example, helium molecules can pass through a membrane significantly more easily than carbon dioxide molecules. The driving force for this separation is provided by a pressure difference across the membrane.

This requirement for a pressure differential requires the use of a compressor on the CO_2+He stream coming from the solar calciner. Compression is electrically expensive, although the consumption can be reduced if the gases are cooled first. To prevent the membrane getting clogged, good-quality filtration and/or electrostatic precipitation prior to the membrane is also required.

Membrane technology is commonly used for increasing He concentrations in gas streams from <5% to 90–95%. Pressure swing adsorption (PSA) technology is used for increasing that purity up to 99.9999 vol% in some cases. Both technologies require compression of the feed gas in order to operate [8], [9]. It is noted that, in a 700 °C system, the helium concentration will be 97% minimum and thus within the range of PSA separation rather than membrane separation. Both methods require compression of the inlet gases to provide a driving force. In the PSA system the CO_2 is adsorbed and the helium leaves at the high pressure whereas in the membrane system the CO_2 is produced at high pressure and the helium at low pressure. Since there is significantly more helium than carbon dioxide, more energy can be recovered by expanding the helium stream than the CO_2 stream.

Several stages of PSA may be required to achieve a high purity. This has knock-on effects on the capital and operating cost of the system for this pilot plant and at larger scales, too. To reduce the energy penalty, the necessary pressure in the PSA system can be reduced by relaxing the constraints on the degree of separation required. For this analysis it was assumed that the gas entering the calciner is 1 vol% CO_2 (denoted lean helium), and it leaves at equilibrium conditions (denoted rich helium). The pressure requirement for the PSA is assumed to be 6 bara. This is significantly less than the 33 bara pressure difference suggested for PSA separation of H_2 and CO_2 which is a good proxy given the small molecule size of hydrogen [10].

A basis of 1 kg/h $CaCO_3$ calcined was taken. The energy required for the calcination reaction is 494 W [6]. A stream of 467 mol/h lean helium allows the partial pressure of CO_2 at the calciner exit to be at the (optimistic) equilibrium value at 700 °C.

This stream, when cooled to 50 °C, has a volumetric flow rate of around 12.7 m^3/h. Using a correlation it is possible to calculate the compression duty [11]. This is found to be 921 W, rising to 1150 W when an 80% efficiency is taken into account. A similar value of 1.15 hp was found using an alternative correlation.

Reducing the concentration of CO_2 in the lean helium reduces the compression requirements. For 0.1 vol% CO_2, the compressor duty (including efficiency loss) falls to 824 W excluding efficiency losses; at 0% CO_2 the value is 798 W (321 mol/h He). This most optimistic value of 798 W is taken forward for the next part of the analysis.

The maximum efficiency of a CSP plant is calculated as the product of the Carnot efficiency at the receiver temperature and the receiver efficiency under infinite solar concentration at that temperature. At 700 °C, this maximum efficiency is 50%. Thus, to generate the 798 W of electricity for running the compressors, 1596 W of primary solar energy are required. Since 494 W of solar energy is required for the calcination of the 1 kg/h $CaCO_3$, a minimum of 2090 W solar energy is required in total. Since only 494 W of this energy can be stored, the efficiency of the process is currently 24%. This does not take in to account any second-law inefficiencies in the power cycle or that an infinite concentration cannot be achieved at the receiver. Nor does it take in to account any energy penalty associated with recovering the helium in the CO_2 stream post-PSA, which could easily be at least 5 vol% [10].

It is noted that a Demonstrator Plant, at larger scale, must compress or liquify the CO_2 for storage over, say, 1 day, and would recover the energy by expansion, so that some non-condensible diluent may be used. In such a plant, the diluent may be in the range of 0–10% in the gas sent to storage to meet CO_2 typical compressor specifications. This would reduce the energy required to be expended in the PSA system on the high concentration CO_2 side.

3.1.2. Heating Costs

Another energy demand in the helium plant is the heating of the gas which enters the reactor. This can be done either in the reactor itself or beforehand. The basis of 1 kg $CaCO_3$/h was continued for the calculation of heating costs.

It can be assumed that in such a plant, a degree of heat integration is performed between cold and hot streams. However, it is difficult to reduce the minimum temperature difference in a low-pressure gas-gas heat exchanger beyond around 100 °C without investment in very large heat exchangers. Thus, a minimum temperature difference of 100 °C is assumed, and that only heating of the pure helium from 600 to 700 °C is required. This requires 2.07 kJ/mol; at 321 mol/h He this is equal to 185 W and reduces maximum plant efficiency when using PSA to 21.7%.

3.2. Calcination in steam

Clearly, the electricity demand of the gas separation membrane units dominates the energy requirement of the calciner system. It appears to be lower in the case of cryogenic separation, but this requires the use of a capitally- and operationally-expensive refrigeration process. This can be avoided by using steam as the diluent, as it can be easily separated by cooling and subsequent condensation of steam at temperatures above ambient. A diagram of the overall process is shown in Figure 6.

It was assumed that the P_{CO2}/P^*_{CO2} would reach 0.9 by the end of the counter-current reactor, something which was achieved by varying the steam input rate. To allow the use of conventional solar receivers, the steam entering the reactor was assumed to be at 700 °C. The reactor was assumed to be adiabatic, with the solids preheated to 100 °C by the reactor exhaust gas after it

has passes through the heat exchanger, and then heated up to 700 °C by the steam. The minimum temperature difference across all heat exchangers was 50 °C. Heaters are required each side of the heat exchanger on the pure steam side: a) to raise the stored water temperature from 25 °C to 100 °C and partially vapourise it; and b) to raise the temperature of the steam from the heat exchanger outlet temperature to 700 °C. The energy input to the first heater was determined by the amount that could be recovered by the heat exchanger. There is a cooler of the H_2O/CO_2 side after the heat exchanger, bringing the temperature down to 75 °C (i.e. ambient + 50 °C).

Sticking to the 1 kg/h example, 495 W is required to calcine the limestone. An iteration to achieve the correct steam flow to lead to the P_{CO2}/P^*_{CO2} = 0.9 condition was calculated to be 9 kg/h, with an exit temperature of 685 °C. The total energy required to heat and vapourise this steam was found to be 5437 W. Some of the 5655 W of cooling duty was used to heat the limestone to 100 °C (temperature at hot end of cooler minus 50 °C). Overall, the efficiency of this process was determined to be 8.8%.

It should be noted that, in addition to the processes shown in Figure 6, the hot CO_2/H_2O coming out of the calciner will have to be de-dusted to protect the heat exchanger and other downstream equipment.

Some analysis was performed using a Calix model of a co-current calciner. The wall and particles were held at 685 °C throughout the reactor, and the model was run to see how the extent of reaction would vary with space-time when a 9:1 ratio of H_2O:$CaCO_3$ (as determined above) was injected. After 170 seconds, the limestone was 98% calcined; after 60, it was 87%.

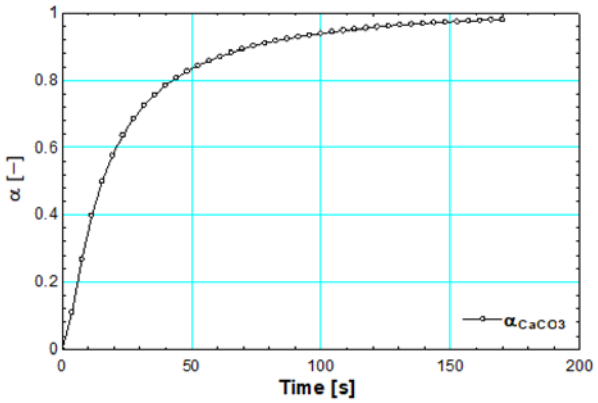

Figure 5: Extent of calcination of limestone at 685 °C in a co-current stream of 9:1 (wt) H_2O:$CaCO_3$, according to the GRPM model explained later.

Assuming a particle agglomerate terminal velocity of around 0.1 m/s (see Section 7.3), counter-current operation and that the steam is travelling at 0.05 m/s, a residence time of 60 seconds can be achieved by a 3 m-high flash calciner. However, the need to inject 9 kg/h steam at 700 °C (a volumetric flow rate of 40.0 m^3/h) means that the reactor's cross section would have to be 0.22 m^2. If the reactor is cylindrical, its diameter must be at least 0.53 m. The cross-section would scale linearly with the amount of sorbent injected, and thus the rate of energy storage; the relationship is 0.45 m^2/kW, so a reactor capable of storing 1 MW would have to be nearly 24 m in diameter under these conditions; this would be impractical.

If this design were to be pursued, a compromise particle size would have to be found. Higher steam velocities could be achieved with larger particles, but the reaction may be hindered by intra-particle heat transfer, which has been shown to be negligible only for particles below approximately 90 µm.

Scaling up the process to a commercial scale will put some of the capital cost in to perspective. For example, running at 1 kg/s (i.e. 3600 times larger than discussed above) can store 1.8 MW of energy in the form of CaO. A heat exchanger with a duty of 17.2 MW would be required for this purpose, and since both sides are atmospheric pressure gases, an overall heat transfer coefficient of 20 $W/m^2.K$ is suitable. The mean temperature difference is close to 50 °C across the entire heat exchanger, so a surface area of around 17 200 m^2 would be required.

Using cost correlations [12] and the Chemical Engineering Process Cost Index (2002 = 395.6 [13]; 2018 = 591.5 [14]), the installed cost of a heat exchanger would be around 3.46 M€. Assuming the equivalent of 3000 hours' operation at full load for 20 years, the heat exchanger will transfer 186 000 GJ/y, or 3.72 million GJ over its lifetime, at a cost of around 0.93 €/GJ. However, the amount of energy transferred in the heat exchanger is much larger than that converted to chemical energy stored in lime; performing the capital cost of the heat exchanger in terms of €/GJ stored, the cost is 25.5 €/GJ. Note that current European costs of gas are around 8.6 €/GJ [15]. This analysis does not take in to account any of the other process units required, such as heaters (i.e. solar receivers) and coolers, let alone the solar field. Given a natural gas CO_2 intensity of 0.056 t CO_2/GJ, the cost of CO_2 abatement of building this heat exchanger (excluding operational costs) rather than burning gas is 301 €/t CO_2.

The impractical reactor requirements, coupled with the low efficiency (<10%) make this process unattractive for energy storage.

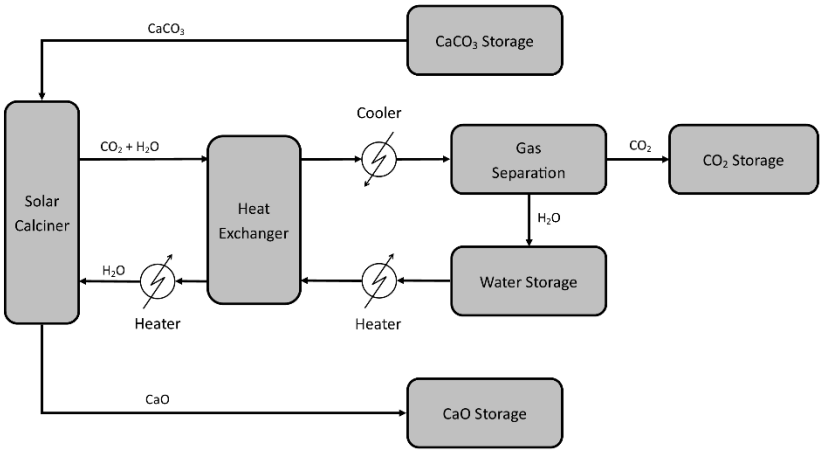

Figure 6: Solar calcination using steam as a diluent

3.3. The kinetics of calcination

So far, only the thermodynamics of calcination has been discussed. The kinetic rate of calcination is just as critical when designing a commercially-viable process. The rate is dependent on the kinetic constant, which manifests in different ways in different models. However, for calcination it is generally a function of the partial pressure of CO_2, the equilibrium pressure of CO_2 and the absolute temperature. An example relationship is [16]:

$$\frac{d\alpha}{dt} = k = Ae^{-\frac{\Delta E}{RT}}\left(1 - \frac{p}{p^*}\right)^{\gamma}$$

Here, α is the extent of calcination of the limestone (mol/mol), k is the kinetic rate constant (1/s), A is the pre-exponential constant (1/s), ΔE is the activation energy of calcination (J/mol), p is the partial pressure of CO_2 (Pa), p^* is the equilibrium partial pressure of CO_2 (Pa) and γ is a constant taken in this report to be equal to 1. It should be remembered that p^* is itself dependent upon the absolute temperature, and thus the only two independent variables influencing the kinetic constant are the actual partial pressure and the absolute temperature.

Criado et al. give the values of *A* and *ΔE* to be 4.43*10^7 /s and 1.87*10^5 J/mol [17]. The part in parentheses with a dependence on the actual and equilibrium partial pressures is known as the thermodynamic term, and the product of the exponential and pre-exponential terms is known as the Arrhenius term.

The kinetic constant of calcination can be calculated for a number of different scenarios. Some are shown in Table 2. Note that, despite the relatively high thermodynamic term for the scenarios under 900 °C, the Arrhenius term is very small (<0.1), meaning that the overall rate is also small. For example, calcination at 1% CO_2 at 700 °C proceeds at around 20% of the rate of calcination at 900 °C under 1 atm CO_2, despite the latter having a lower thermodynamic driving force. However, the thermodynamic driving force should not be underestimated as an important factor. For example, to gain the same rate at 1 atm CO_2 as is possible at 0.01 atm CO_2 at 900 °C, the temperature must be raised to 943 °C, a significant difference.

Table 2: The kinetic rate constant, k, for different combinations of temperature and p_{CO2}

Temperature	p_{CO2}* (atm)	p_{CO2} (atm)	Arrhenius term (/s)	Thermodynamic term	k (/s)
700	0.030	0.01	0.004	0.664	0.003
800	0.212	0.01	0.035	0.953	0.034
900	1.075	0.01	0.211	0.991	0.209
900	1.075	1	0.211	0.070	0.014
910	1.246	1	0.248	0.198	0.049
920	1.441	1	0.291	0.306	0.089
930	1.662	1	0.340	0.398	0.135
943.3	2.002	1	0.417	0.501	0.209

The implications for flash calciners are severe. Unlike processes such as fluidised beds where the residence time is determined by the rate of material addition and removal, the residence time in a flash calciner is highly dependent upon particle size and reactor vertical length. For particles <100 μm, a reactor of a few tens of metres is necessary to attain a suitable residence time. Longer residence times require taller reactors, and so longer residence times become less practical and more expensive. A fast rate of reaction allows for shorter reactors for a given extent of reaction, providing enough heat can be supplied. Furthermore, shorter residence times reduces sintering, enabling the material to be more reactive next time it passes through the calciner.

These kinetic rate constants are proportional to the rate of reaction given otherwise equal conditions, so the residence time of sorbent at 700 °C in 1% CO_2 would need to be around 30 times longer than at 920 °C in 100% CO_2, and thus the reactor 30 times longer too (excluding length needed for heating the sorbent).

In Deliverable 3.2, the GRPM model was introduced and is summarised below:

$$k\left(T, p_{CO_2}, p_{H_2O}\right) = k_A(T)\left[1 - \theta_{CO_2}\left(T, p_{CO_2}\right)\right]^{N_\nu}\left[1 + \theta_{H_2O}\left(T, p_{CO_2}, p_{H_2O}\right)\Delta(T)\right]\left[1 - \frac{p_{CO_2}}{p_{CO_2,eq}(T)}\right]$$

$$k_A(T) = 0.021\ exp\left[-\frac{130}{RT}\right]$$

$$\theta_{CO_2}\left(T, p_{CO_2}, p_{H_2O}\right) = \frac{\frac{p_{CO_2}}{P_{CO_2,eq}(T)}}{1 + \left[\frac{p_{CO_2}}{P_{CO_2,eq}(T)} + \frac{p_{H_2O}}{P_{H_2O,sat}(T)}\right]}$$

$$\theta_{H_2O}(T, p_{CO_2}, p_{H_2O}) = \frac{\frac{p_{H_2O}}{P_{H_2O,sat}(T)}}{1 + \left[\frac{p_{CO_2}}{P_{CO_2,eq}(T)} + \frac{p_{H_2O}}{P_{H_2O,sat}(T)}\right]}$$

$$p_{CO_2,eq}(T) = 4.137\ 10^7 \exp\left\{-\frac{20474}{T}\right\}$$

$$p_{H_2O,sat}(T) = 3.33\ 10^6 \exp\left\{-\frac{12594}{T}\right\}$$

$$\Delta(T) = \ 14150\ exp\left\{-\frac{6014}{T}\right\}$$

Here, k and k_A are the temperature-dependent and temperature-independent velocities of the reaction front measured in m/s, R is the ideal gas constant (8.314 J/(mol.K)), T is the absolute temperature in K, all pressures and equilibrium pressures are in bara, and N_v is equal to 1. Example velocities are shown in Table 3. It is clear that the effect of temperature is less significant than in the kinetic model given above – the difference between 700 °C and 900 °C at 0.01 atm the ratio of rates is around half. Furthermore, the effect of partial pressure is greater in the GRPM than in the model above. Having said that, the velocity at 900 °C in 1 atm is higher than that at 700 °C in 0.01 atm, and the velocity at 920 °C is seven times larger.

Table 3: The reaction front velocity, k, for different combinations of temperature and p_{CO2}

Temperature	p_{CO2}* (atm)	p_{CO2} (atm)	Θ_{CO2}	k_A (nm/s)	k (nm/s)
700	0.030	0.01	0.251	2.21	1.10
800	0.212	0.01	0.045	9.87	8.98
900	1.076	0.01	0.009	34.18	33.55
900	1.076	1	0.482	34.18	1.25
910	1.247	1	0.445	38.25	4.20
920	1.441	1	0.410	42.73	7.72
930	1.662	1	0.376	47.65	11.85

Furthermore, the absence of a requirement to heat a dilution gas means that the only energy not used for reaction is that needed to heat the limestone to 920 °C. This is around 1030 kJ/kg compared with a reaction enthalpy of 1780 kJ/kg; this results in a process efficiency of 63%, significantly higher than those calculated for the 700 °C.

3.4. Conclusions

The analysis presented above has three main findings:

- Use of gas separation methods which use a pressure as a driving force are highly energetically expensive (and thus inefficient) because of the need to use electricity to power the compressors.
- Calcining at 700 °C at atmospheric pressure requires the use of a large amount dilution gas to reduce the carbon dioxide pressure to less than 3 kPa. Heating and treating this dilution gas requires large amounts of energy, even when a significant amount of heat integration is applied. This leads to inefficiency. Due to the low density of the energy to be transferred, the capital cost of a suitable heat exchanger alone would cost more than €25/GJ chemical energy stored in the lime.

- The kinetics of calcining at 700 °C are slow even in 0% CO_2. Similar rates can be achieved when calcining in pure CO_2 at 900 °C; rates an order of magnitude higher can be achieved at 920–930 °C and remove the need for gas separation. The absence of the need to heat the dilution gas means the efficiency is significantly higher.

Table 4: Simple (ex. solar) efficiencies of different process concepts

Process temperature and atmosphere	Simple Efficiency	Main inefficiency
700 °C, Helium	22%	Generation of electricity for pressure swing adsorption system
700 °C, Steam	9%	Raising steam at 100 °C
920 °C, CO_2	63%	Heating of limestone from ambient

The simple efficiencies (i.e. without solar losses or losses from the process units themselves) are shown in Table 4. It is noted that in an operating system, the actual heating loss for the systems may be significantly reduced by storing the $CaCO_3$ from the carbonator at about the carbonation temperature. Given these findings, the need for fast kinetics as well as the desire for efficient energy storage leads to the conclusion that the calciner should operate in 100% CO_2 at process temperatures in excess of 900 °C.

4. THE PHYSICS OF SOLAR POWER

Although most industrial processes are powered by solar power indirectly via fossil fuels, biofuels and electricity, few are powered by direct solar power. Concentrated solar power (i.e. electricity generation) has developed quickly over the last few years and technical and scientific advances have reduced the cost of harnessing this form of energy.

Solar energy comes as radiation, which has natural laws governing it. One of the most important is the Stefan-Boltzmann Law, which states that the amount of energy radiating from a surface of a black body (the black body radiant emittance) is:

$$q_{bb} = \sigma T^4$$

Here, q is the flux per unit area ($W.m^{-2}$), σ is the Stefan-Boltzmann constant ($5.67*10^{-8}$ $W.m^{-2}.K^{-1}$) and T is the absolute temperature (K). However, black bodies are rare in nature and most bodies emit a fraction of the black-body radiant emittance. This fraction is denoted as the emittance of the body, ε, and such bodies are called grey bodies. It can be placed as another factor in the right-hand side of the equation above to provide the grey body radiant emittance:

$$q_{gb} = \sigma \epsilon T^4$$

While bodies emit radiation, they can also absorb it. A black body absorbs all radiation incident upon it, and grey bodies absorb only a certain fraction. The ratio of the amount absorbed by a body to the amount incident upon it is the definition of the absorbance α. The rest of the radiation (the fraction 1-α) is either transmitted through the body or reflected.

PART TWO: SOLAR CALCINER DESIGN & ANALYSIS

5. DESIGN ITERATIONS

This section of the deliverable documents the various reactor designs which have been considered and analysed by Work Package 3. They are presented in close to the order in which they were analysed.

5.1. Design 1: Irradiated Tube

This design is shown in Figure 7. It comprises a cylindrical reactor tube down which sorbent is passed. Heliostats located all around the reactor reflect sunlight along the length of the reactor, heating it up. This heat is then transferred to the sorbent inside.

This is the most simple solar powered CFC design, as it simply replaces the fuel furnace with irradiated sunlight. However, a quick analysis suggests that a reactor that has a 50 mm outside diameter and an 8 m height will lose a significant amount of energy through re-radiation. Assuming it is made of a polished stainless steel with an emissivity of 0.19 and must be held at 950 °C to enable process temperatures in the region of 920–930 °C, it will emit around 30 kW to the environment. Furthermore, the steel will have an absorptance of a similar value to its emissivity. With an energy requirement of around 40 kW (30 kW from losses and 10 kW for processing the limestone), a solar field with a capacity of around (40/0.19=) 210 kW would be required; this is an efficiency of 4.8%.

It is important to note that most materials have similar absorptance and emissivities. Thus, replacing the steel with a material with a higher absorptivity would almost certainly lead to a higher emissivity, too – this means that the energy balance would be relatively unchanged, and certainly not changed enough to counter-act the hugely inefficient design.

This analysis shows that the losses from an uncontained hot tube are intolerable for a design which should be as efficient as possible. As such, it is necessary to insulate the tube and provide the solar radiation in a different manner.

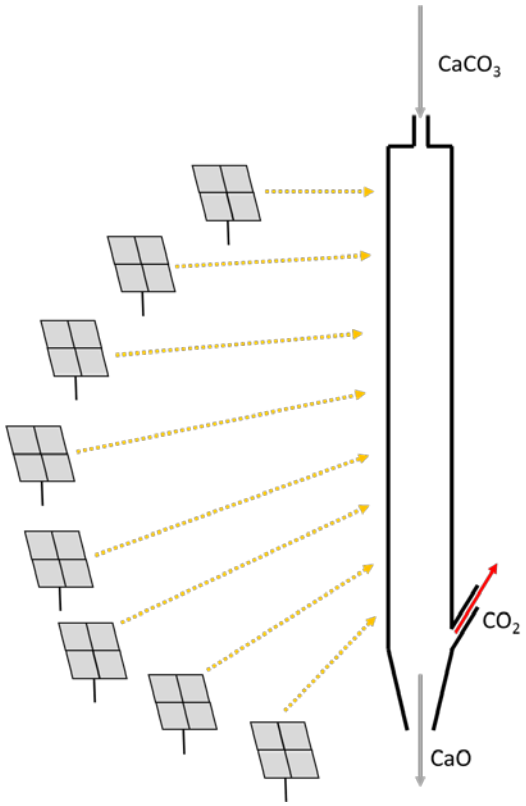

Figure 7: Irradiated tube reactor design

5.2. Design 2: Heat pipes

Heat pipes are efficient tools for transferring large quantities of heat. They contain a substance in vapour-liquid equilibrium (VLE). Applying heat causes some of the liquid to vaporise and travel in the tube. The gas passes to the colder end of the heat pipe and condenses, releasing its latent

heat of vaporisation. Heat transfer between surfaces and a fluid is significantly easier when phase change is used; thus, heat pipes can transfer significant amounts of heat with no moving parts.

At the temperatures of calcination it is likely that a molten metal would be used as the fluid. At temperatures above 900 °C as required within the calciner, sodium would be a suitable choice.

A design for a calciner powered using heat pipes is shown in Figure 8. Heliostats shine on to receivers attached to the end of each heat tube. The heat tubes are angled slightly upwards in to the calciner to facilitate the flow of liquid down towards the receiver and gases upwards towards the calciner. The heat pipes, in fact, pass right through the calciner and in to a heat exchanger containing pipes for CO_2 and for a heat transfer fluid (HTF). In calcination mode, the majority of the heat is emitted in the calciner. However, the hot CO_2 generated in the calciner passes through a filter and the CO_2/HTF heat exchanger. The now hot HTF passes through a turbine to generate a moderate amount of electricity.

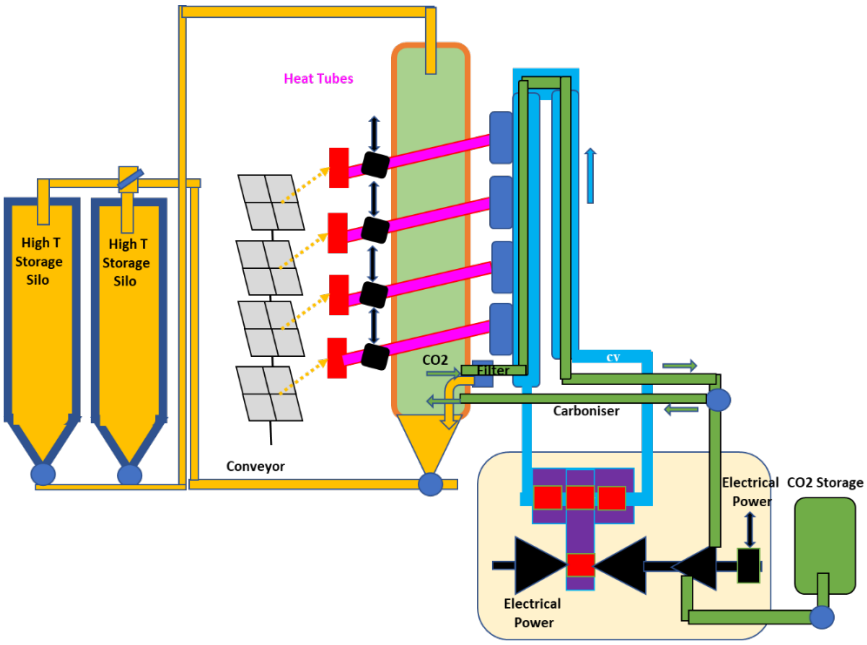

Figure 8: Design 2a: Calciner design with single heat pipe array for calcination and carbonation

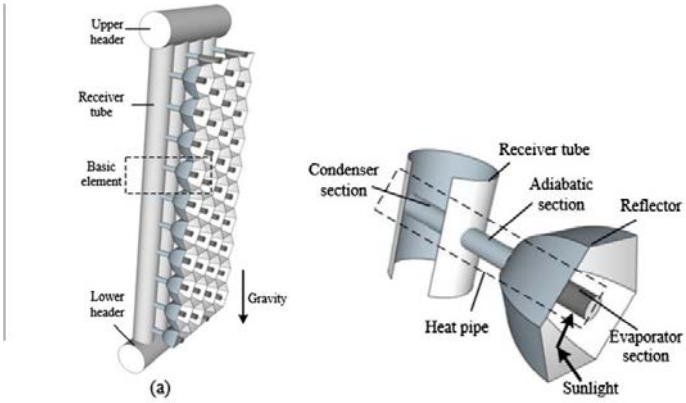

Figure 9: The heat pipe receiver of Liao & Faghri [18]

The design of this reactor allows it to operate as a carbonator, as well. As previously noted, it is very unlikely that both calcination and carbonation will be required at the same time. During carbonation, solids pass down the reactor and come in to contact with CO_2 that is pumped in from storage. The carbonation reaction heats up the solids and gases. A super-stoichiometric amount of CO_2 is injected, with the unreacted gas passing through the heat transfer fluid as in the calcination case. Furthermore, the heat pipes transfer heat from the carbonator to the heat transfer fluid, increasing the electricity output.

There are few constraints on the size or length of heat pipes, and so the number and heat output of each heat pipe could be determined during detailed design. This would be performed in conjunction with the design of the solar receivers. There are some designs which already exist which could be used, such as that of Liao & Faghri, which is shown in Figure 9 [18].

A major issue for this process is that heat pipes work best within a given temperature range. Furthermore, the fraction of heat which could go straight to the HTF in the calcination case is difficult to control; during carbonation, there would be the same issue at the receiver end. For this reason, an adapted design was considered, which involved two sets of heat pipes – one from

the solar receivers to the calciner-carbonator, and one from the calciner-carbonator to the HTF heat exchanger. This is shown in Figure 10. This adaptation uses an annular reactor with a beam-down cavity in the centre to capture the radiation.

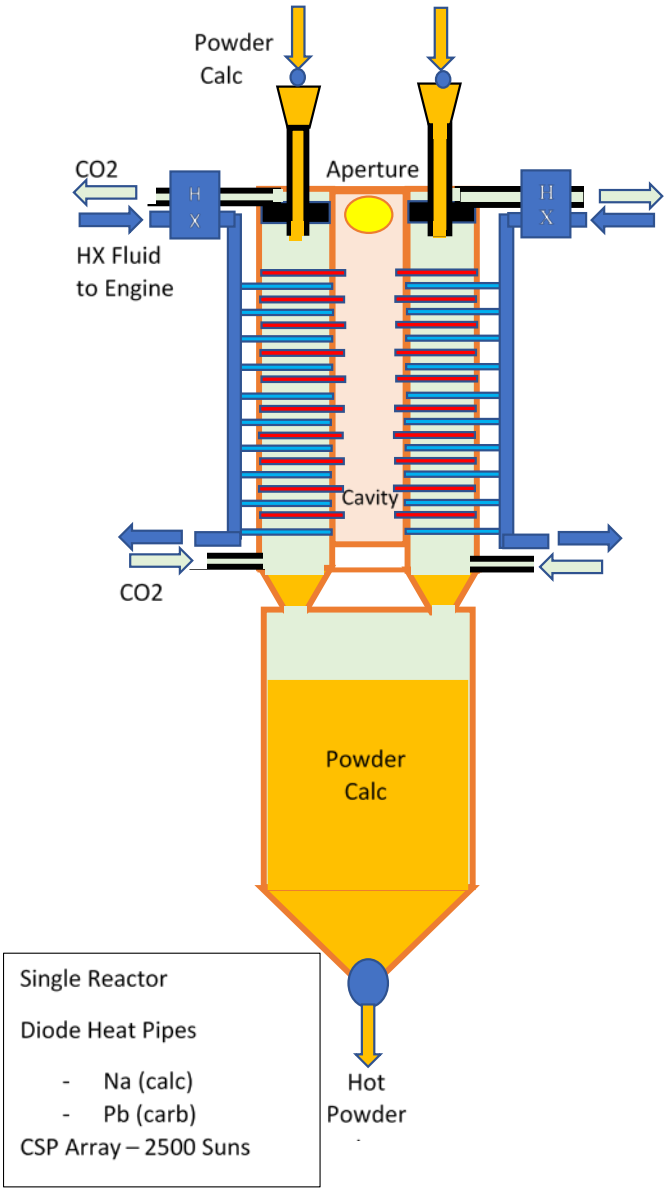

Figure 10: Dual heat pipe calciner design

During the design and discussions several more issues were raised, which pertain to both this design and the original heat pipe design. Firstly, CFCs do not have much deposition on their vertical walls because the walls are hotter than the fluid inside; thermophoresis significantly reduces particle-wall interactions. The concept of several immersed heating elements within a CFC is practical, having undergone analysis during LEILAC. In the case of heat removal from the unit during carbonation, the opposite is true; thermophoresis attracts particles to the reactor wall. The near-horizontal surfaces on the heat pipes would also suffer from this issue, attracting the particles. in the lime industry, it is known that the carbonising particles bind together through Ca-CO_2-Ca bridges. Thus, fouling is a problem during both calcination and carbonation, but certainly to a larger extent in the latter; the non-vertical surfaces would suffer from this much more than vertical ones.

Another issue with this design is that it is very complex, with two sets of heat pipes. It would be difficult to build a scaled-down version for testing, and at large scale advice from solar power experts was that it would be difficult to design the aperture so that the heat was well-distributed to the heat pipes due to shading and limitations about the flux profile within the cavity.

For all of these reasons, the heat pipe design was abandoned.

5.3. Design 3: Hot CO_2

A design was submitted by University of Seville for consideration which aimed to avoid the issues around getting high-temperature radiation in to the reactor. In this reactor design, a volumetric receiver made with a ceramic foam is irradiated. The high surface area and high absorptance of the foam heats it up. CO_2 is blown through the foam where it heats up due to forced convection. The CO_2 is then conveyed in to the reactor where it heats up the limestone and passes on heat to effect calcination. The design is shown in Figure 11.

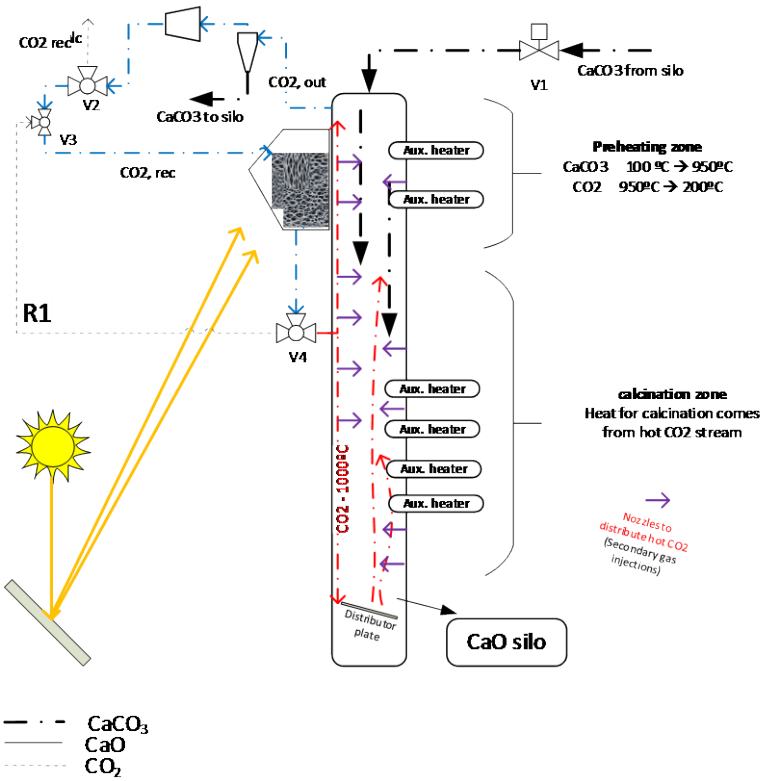

Figure 11: The 'hot CO_2' reactor design

Some basic calculations can be performed to determine the amount of CO_2 needed to perform calcination. The 1 kg/h $CaCO_3$ basis is taken again. To heat calcium carbonate from 100 °C to 920 °C and effect complete calcination requires 3.07 MJ/kg. Around three-quarters (74%) is needed for calcination. It is assumed that the energy can be passed to the limestone from any CO_2 at a temperature higher than 900 °C, and that the maximum temperature attainable in the CO_2 coming out of the receiver is 1200 °C. The heat that can be imparted by CO_2 as it cools from 1200 °C to 900 °C is 373 kJ/kg; thus, at least 8.2 kg CO_2 is required per kilogram of $CaCO_3$ that has to be heated and calcined.

The radiative losses of a receiver which generates CO_2 at 1200 °C could be particularly large. Assuming a 50 °C driving force for convective heat transfer between the receiver and the CO_2 leaving it, the receiver would have to be at around 1250 °C. Due to the dependence on the fourth

power of the absolute temperature, the radiance of the receiver would be twice that at 1000 °C. Measures to reduce this can be taken, such as reducing the surface area of the receiver or placing it in a cavity, but this is only possible to an extent and is likely to have been pushed close to the limit even for receivers at 1000 °C.

Turning to the flow rate of CO_2 required, it is rather large when expressed in volumetric terms – around 18 m^3 at 900 °C. Considering the electric calciner design (given below in Section 6) with an inside diameter of around 45 mm and a throughput of only 10 kg/h, 50 L/s CO_2 will have to be passed through the reactor to achieve this – it would have a velocity of 25 m/s. That said, increasing the diameter to 450 mm would allow a velocity of 0.25 m/s, which would be acceptable. Another possibility with this design is to introduce the hot CO_2 gas in various locations. This would reduce the amount of gas used at the top of the reactor.

The design requires the re-circulation of the CO_2 to transfer the heat. One major hurdle is that the CO_2 must be conveyed, potentially by fans but potentially by blowers if more pressure driving force is required. Fans capable of operating up to 1200 °C exist (and provide a 0.2 bar pressure increase [19]) it may not be possible to find the valves and other such equipment which can operate at those temperatures. Disregarding that last point for a moment, a fan which increase pressure by 0.1 bar for the 50 L/s CO_2 would need around 498 W, excluding inefficiencies. This is approximately equal to 1.5 kW primary energy when assuming a solar Rankine cycle can run at an efficiency of 0.33. This is relatively low compared with the calcination and heating of around 7160 W for a 10 kg/h system; it is equivalent to an efficiency de-rating of 17%.

Furthermore, such a system is likely to involve temperature losses. On a large scale these can be minimised by insulation and a low surface area-to-volume ratio. Given the 300 °C rise in temperature and, assuming a roughly stable heat capacity of CO_2, the temperature of the gas falling to 800 °C in the post-calciner processing section would lead to a 33% increase in energy use, equivalent to a 25% reduction in efficiency. This energy loss may be forced upon the process by the maximum temperature that can be withstood by some of the equipment.

5.4. Design 4: Direct irradiation

Previous designs have used a heat transfer medium (Design 3) or a radiating surface (Designs 1 & 2) to pass heat to the limestone. The concentrated sunlight heats up the medium or surface, which then re-radiates to the sorbent. This design removes that intermediary and places the sorbent in direct concentrated solar radiation. The high intensity of the solar flux heats the sorbent extremely quickly, raising the temperature and effecting calcination.

In this 'Direct Irradiation' [of the sorbent] design as shown in Figure 12, sorbent passes through a beam-down receiver from the top. The radiation is quite focused compared with the size of the receiver. By injecting the sorbent at an angle and producing a plume in the centre of the receiver, the sorbent is irradiated and heats up. Since the irradiation is direct, most of the walls of the receiver are likely to stay cooler than they would do otherwise, easing design.

An important consideration throughout all of the design iteration exercise has been to ensure the gas-tightness of the reactor chamber. In this case, it is the same as that which receives solar radiation. In the designs shown until now, the use of an intermediate has precluded the need to keep the solar receiver gas-tight. However, with limestone now calcining in the receiver it is necessary to control that environment. A typical method to do this is to use a transparent window across the aperture so that light can enter but gas cannot. The conventional material for this task is quartz, which is highly transparent. However, its properties make gas-tightness difficult, in particular with respect to thermal expansion. Its thermal expansion coefficient is

lower than that of steel. Any gas-tight connection would come under serious stress as the reactor heated up, with the possibility that the window would crack. Complex design would be required to make the reactor gas-tight over a range of temperatures.

Another issue with direct-irradiation calciners is that the particles often foul the window. This reduces the transparency of the quartz and leads to inefficiency and also a higher window temperature. Some solutions have been proposed, such as using a gas curtain to keep particles from the window. This is technically possible but comes with inefficiencies – in this case, the CO_2 used in the curtain would have to be fully dedusted and compressed. This has a similar effect to introducing a recycle loop, albeit a small one.

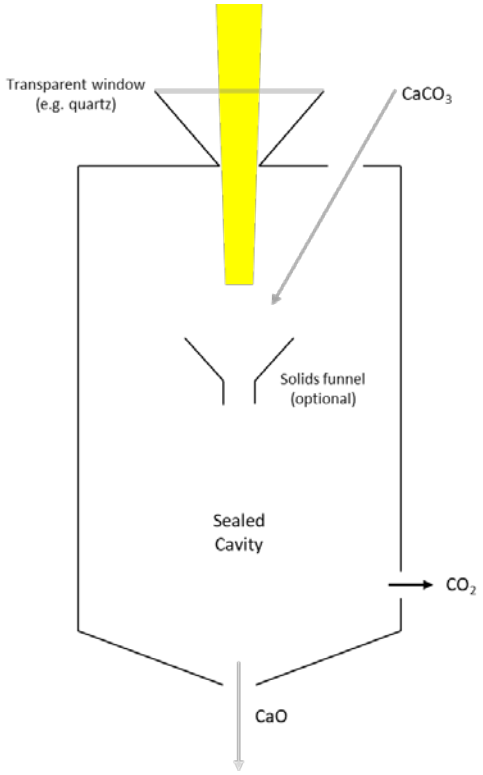

Figure 12: The 'Direct Irradiation' solar calciner design

One benefit of using an intermediate is that it tends to smooth out the radiative heat flux. For Design 3, the CO_2 blends with itself so any hotter pockets will heat up cooler ones. A cavity tends to smooth out temperature differences as the wall irradiates itself. This reduces the risk of over- and under-heating sorbent as it passes through different parts of the reactor. Design 4 does not benefit from this phenomenon because the sorbent is exposed to the solar radiation as it enters the cavity. The radiation from each heliostat will enter the reactor on a slightly different trajectory; although the secondary reflector can reduce this effect slightly, there are likely to be hotspots and coldspots throughout the cavity.

Excessive sintering of the sorbent may occur in the hotspots, whereas in the coldspots incomplete calcination may occur, reducing the energy storage efficiency. Furthermore, particles in the upper layer will shadow particles further down, reducing their ability to absorb radiation.

Some solutions to these problems exist. Firstly, introducing turbulence in the solids flow by injecting gas with the solids may improve powder mixing. Although this does not affect the hot- and cold-spots per se, it would reduce the heterogeneity of the powder and thus a particular particle would be more likely to experience more hot- and cold-spots that it would otherwise.

Another solution is to alter the reactor design so that the cavity is conical and the particles move in a helix down through the reactor. This distributes the powder more homogeneously in the plane perpendicular to the radiation's direction as well as making it easier to heat particles at the bottom of the reactor, since the upper layers are pushed to the side of the cavity.

There were concerns that the residence time within the solar beam would not be long enough to cause full heating and calcination. To address this issue, it was suggested to use a splash plate or funnel located in the flow of sorbent to increase the residence time. This would break the particles' falls and hold them up in the reactor, providing some extra seconds to achieve the necessary irradiation. The exact design would be based on the extra time needed and reactor and fluid simulations.

Numerous attempts have been made to build a direct irradiation reactor, as shown in Section 15.2 in the Annex. Generally, performance is lower than predicted and there have been some issues with fouling of the aperture window.

5.5. Design 5: Indirect irradiation

The difficulty of designing and operating a direct irradiation calciner implies that indirect irradiation, as shown in Designs 1–3, is more likely to succeed despite the inefficiency, at least at the scale of SOCRATCES. The 'Direct Irradiation' design was modified to include a windowless cavity which re-radiates the energy in to the reactor annulus, as shown in Figure 13. This is similar to Design 2b in Figure 10 in that it has a reaction annulus, but it does not contain heat pipes.

This design is rather similar to the existing CFC design except that the reaction and energy supply have been switched around. It may be possible to build one in which the radiation is passed in to the annulus, but to get good distribution around the ring cross-section a complex system of mirrors and/or prisms would need to be used.

As with any cavity reactor, a big challenge is distributing the radiation throughout the cavity. The aperture of a beam-down annular reactor, whilst less problematic than that in Design 4, still presents issues. Firstly, radiation will leave the aperture. If it is assumed that little primary (i.e. solar) radiation escapes, then the radiation passing out of the cavity is that which is radiated from the cavity wall. The intensity of this radiation is dependent on the temperature of the cavity wall and the cross-sectional area of the aperture. As the temperature of the wall increases, the amount of energy leaving the aperture also does; this means less is passing in to the reaction annulus and the cavity becomes less efficient. Thus, there is a balance to be struck with regard to cavity wall temperature. The hotter it is the more energy is emitted from the wall's annular face, but also more energy is emitted, and escapes, from the cavity face too. The aperture should be kept as small as possible, and the minimum size is dictated by the level of focus that can be achieved by the solar field and secondary reflector.

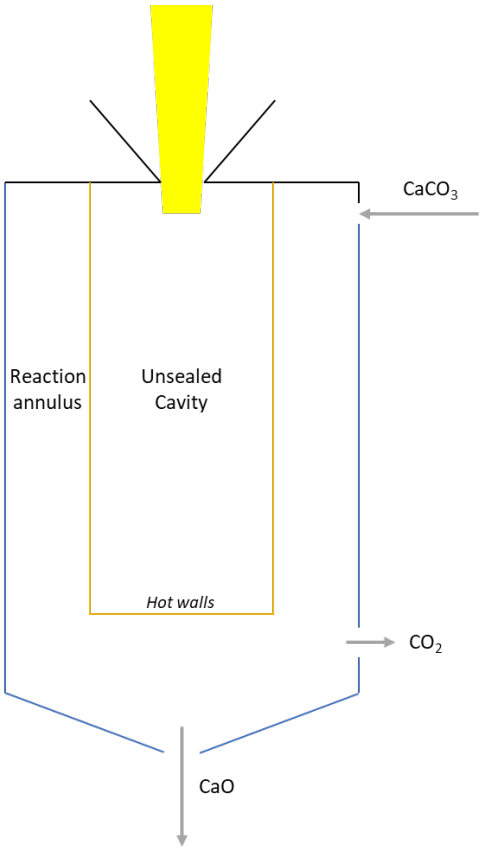

Figure 13: Indirect irradiation solar calciner design

For a given net input of radiation, the more surface area the cavity wall has, the cooler it will be. This is another constraint on the reactor dimensions. Residence times in this reaction are expected to be in the range of 5–20 seconds.

The fact that Design 5 reflects existing CFC designs is beneficial because it means many of the correlations and models that exist for fossil-fuelled versions can be easily adapted for this solar version. In a commercial plant, the height is not a limitation.

5.6. Design 6: Vibrating table

Concerns about the short residence time of particles in a CFC-style reactor led to the development of one final design. Since gravity inflicts a set terminal velocity for a specific particle it is not possible to greatly affect the residence time in a fixed-length reactor. Design 6 omits falling particles altogether to overcome the residence time issue, and is shown in Figure 14. Here, a long vibrating table (or series of them) pass particles or powder through a preheating zone and then under a radiating plate. The radiation causes the powder to calcine. The hot gases generated by calcination pass along the preheating section and out of the system to de-dusting and storage. The powder continues its journey beyond the radiating plate and falls in to a storage system. The radiating plate is the bottom of a solar cavity, and is heated by the concentrated solar energy from the solar field.

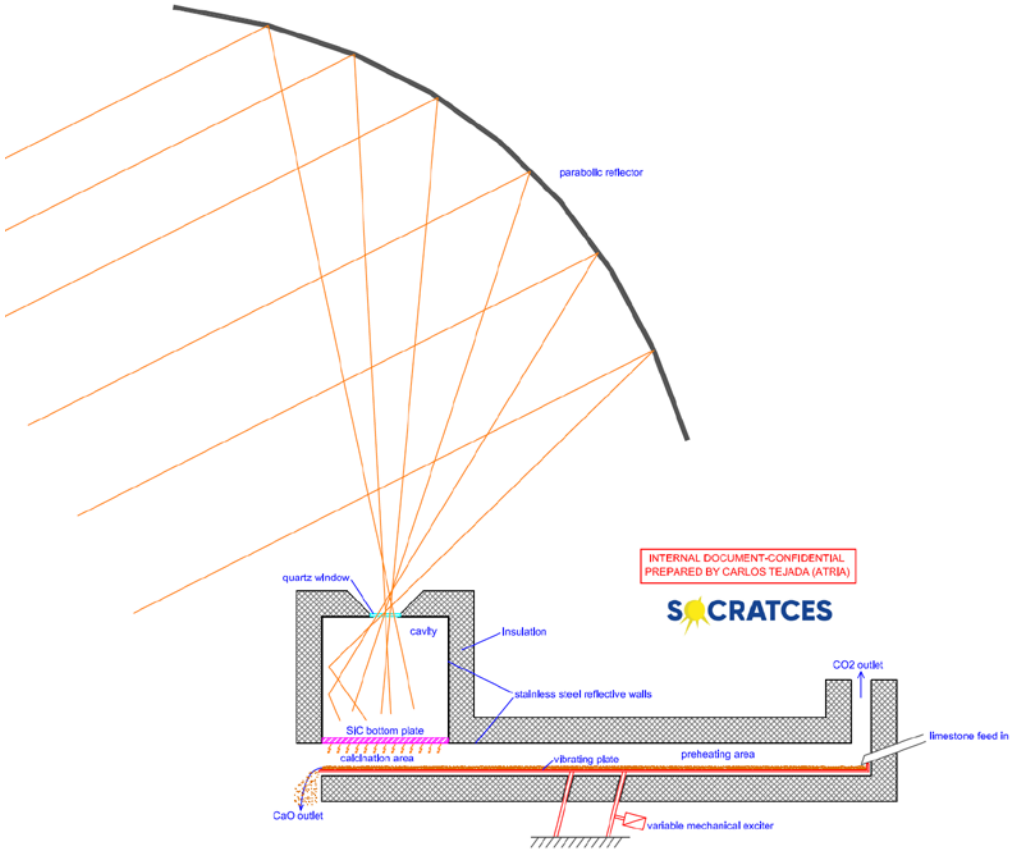

Figure 14: Vibrating table reactor design

The variable mechanical exciter can be manipulated to control the rate of travel down the vibrating plates and thus the residence time of the powder. However, it may be necessary to use particles with a larger average diameter in this design; vibration of powders leads to significant entrainment in gas flows. This would lead to a circulation of powder on the vibrating plates, especially for calcined material which has a lower density. Another issue with vibration is that the particles may have the opportunity to escape the plate; an improvement may be to turn the plate in to a trough, i.e. a plate with sides, to minimise this. However, it may be difficult to prevent this around any joins between plates.

The major problem with this design is that the vibrating plate design is untested, and that it is likely to be difficult to control. Furthermore, it does not meet the requirement of being a CFC-style reactor. The depth of particle bed would be difficult to control, and the less dense CaO particles would tend to rise to the surface, insulating the particles deeper in the bed. Managing to convey enough heat to the lower section of the bed would lead to sintering of the top side of the bed as it heats up to transfer the heat.

5.7. Decision

On reflection, each design has challenges and drawbacks as well as benefits. They are summarised below.

Design 1 (irradiated tube) is the simplest, as it requires no cavity, secondary reflector or other equipment beyond heliostats and a steel reactor. However, the efficiency of such a reactor would be unacceptably low as around 75% of the heat is likely to be lost via re-radiation from the hot tube.

Design 2 (heat pipes) represents a method of reducing the re-radiation losses, since the heat tubes are mostly within the reactor. The use of several individual heat pipes would enable the heat to be more evenly spread throughout the reactor. However, this design is complex because of the number of heat pipes required and the new almost-horizontal surfaces which would be produced inside the reactor, promoting fouling.

Design 3 (hot CO_2) moves away from the CFC design and the provision of radiation in to the reactor by using CO_2 as a heat transfer medium. This allows the use of more conventional volumetric solar receivers, but the temperatures (1200 °C) as well as the volumes of CO_2 required to circulated at high temperature to transfer the heat make this design difficult to implement.

Design 4 (direct irradiation) removes the use of an intermediary gas or surface between the solar radiation and the sorbent. This could lead to a more efficient process, but suffers from the need to design a gas-tight cavity with a transparent window which must be kept free of particle deposits. Furthermore, there are concerns about the homogeneity of the product given the low residence time and particle-particle shadowing.

Design 5 (indirect irradiation) is a beam-down reactor like Designs 2 & 4 but is annular and as such keeps the solar radiation and sorbent separate. It is an inside-out conventional CFC and as such can benefit from a lot of the existing understanding of CFC design and modelling. However, the cavity geometry constraints constrain the length of the reactor and thus the residence time.

Design 6 (vibrating table) removes the CFC aspect of the calciner completely, preferring a horizontally-moving bed of particles which pass under a radiating plate. The bed is vibrated to move it down a shallow slope. This design could work, but the residence time under the plate and the agglomeration of particles is a worry, as well as excessive sintering of the upper layers of the vibrated bed and under-calcination in the lower layers.

Based on the six designs given above, it was decided to move ahead with Design 5 (indirect irradiation). Although it suffers from a short residence time, the analysis which is given later in this document shows that it should be able to calcine to a reasonable degree in the expected residence time.

6. ELECTRIC-SOLAR CALCINER

The solar calciner is of a new design (indirect CFC) and is being operated under conditions unlike those which have been used for either calcium looping or CSP. This means there are a number of uncertainties and unknowns which cannot be entirely addressed before construction. Furthermore, using such a small reactor which is dependent on the intensity of solar radiation from the solar field via the solar receiver makes it difficult to control the quality of the solar-calcined sorbent. This will negatively affect the carbonator's ability to test its design.

The operation of a dispatchable, reliable calciner to complement the solar calciner would provide some relief from these uncertainties, enabling WP7 to collect sorbent and data even during times when solar energy is not available in the quantities required to operate the solar calciner properly.

To be dispatchable, the calciner must use a non-intermittent form of energy. This means it needs to be a fuel or electricity. Although for large-scale, long-term operation it may make sense to use a carbonaceous fuel such as natural gas or biomass, the complexities and capital cost of using these on-site are outweighed by their relatively low expense compared with electricity. Using grid electricity allows the use of relatively cheap electrical elements which give a high degree of control to the conditions within the calciner. The regulations surrounding the use of electricity tend to be easier to adhere to than those about fuels. Together with the complexity of combustion systems, the time to design an electric calciner is likely to be shorter, and thus

put less strain on the project's schedule. For these reasons, the dispatchable calciner was decided to be have an auxiliary electric power source.

For testing, the auxiliary electric power must be able to fully calcine sorbent using electricity in a controlled atmosphere of CO_2 or a mixture of CO_2 and other gases.

7. SOLAR CALCINER DESIGN

Having chosen the indirect CFC as the concept for the reactor, some modelling and detailed literature review was required to determine its size, shape and method of operation.

A model was designed in Excel which 'built' a calciner using the principles of radiative heat transfer and particle terminal velocities. Firstly, the model for heat transfer between a cloud of particles and an opaque plane (i.e. wall) was implemented. It is given in the Annex of this Deliverable. In general, the emissivity and absorptance of the particle cloud are both approximately 0.33.

7.1. Assumptions/data

- To heat up and calcine, the limestone requires ca. 400 & 1860 kJ/kg [6], [20], respectively, equalling 2260 kJ/kg overall.
- The receiver is nominally 10 kW but will have losses via its aperture which are calculated below.
- The whole apparatus is made of stainless steel or silicon carbide (SiC). SiC has an emissivity of around 0.95. It is assumed that the stainless steel will be oxidised on both sides. The emissivity is assumed to be 0.85 [21].
- The emissivity of the particle cloud is determined using the method shown in the Annex.
- Only limestone and CO_2 enter the reactor as a gas-solid mixture.
- The outside of the annulus is insulated by 50 mm superwool at 0.3 W/mK. There are no heat losses anywhere else. It is likely that without the quartz window there will be convective losses from the beam-down cavity but these have not yet been quantified.
- The spherical, pure $CaCO_3$ particles have a monotonic diameter of 7.8 μm. Their aggregation is dictated by the method shown in the annex.
- Intra-particle heat transfer will be instantaneous, given their small size and therefore high surface area-to-volume ratio.

7.2. Energy Balances

There are 5 important fluxes within the reactor:

- CSP hitting the inside of the cavity, Q_{CSP};
- Radiation escaping the cavity via the aperture, Q_{ap};
- Radiation from the outside of the cavity to the particle cloud, $Q_{g+p,cav}$;
- Radiation from the particle cloud to the reactor's outside shell, $Q_{g+p,w}$;
- Conduction through the reactor's insulation to the air, Q_{conv}.

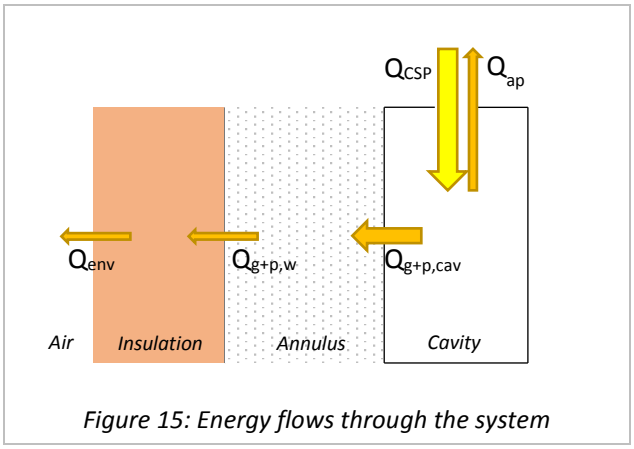

Figure 15: Energy flows through the system

7.2.1. Energy Balance on Cavity Wall

The incoming CSP, Q_{in}, is defined as being 10 000 W. All of this radiation either escapes via the aperture or enters the annulus in which the particle cloud exists. Thus, the sum of these two must equal the 10 000 W coming in, and both are dependent upon the cavity surface temperature, which is assumed to be the same throughout its thickness. The cavity can be treated as a black-body emitter through its aperture, so the amount leaving through that mechanism is

$$Q_{ap} = \pi r_{ap}^2 \sigma \epsilon_{bb} (T_{cav}^4 - T_{env}^4)$$

Here, the environmental temperature is assumed to be 298 K and ε_{bb} = 1. The value of r_{ap} is 0.1 m, which is set by the minimum focus diameter of the solar energy calculated in Task 3.4. Note that if we assume the average incident solar irradiation is 1 kW/m^2 then at 10 kW of radiation delivered and r_{ap} = 0.1 m, the solar radiation concentration ratio is only 80, ignoring any losses before the aperture. This compares with values of 400 [22], 350 [23], 150 [24] and 250 [25] in similarly-sized high-temperature R&D plants. For larger-scale plants, even higher concentrations of up to 600 can be expected [26]. The low concentration ratio of 80 constrains the efficiency of the plant and the temperature that can be achieved within the cavity.

The energy leaving the cavity wall to the particle cloud is

$$Q_{g+p,cav} = \frac{\pi d_{cav} h_{cav} \epsilon_{cav} \sigma \left(\epsilon_{g+p} T_g^4 - \alpha_{g+p} T_{cav}^4\right)}{\alpha_{g+p} + \epsilon_{cav} - \alpha_{g+p} \epsilon_{cav}}$$

The gas and particle temperatures are assumed to be equal at 927 °C, or 1200 K. The ratio h_{cav}:d_{cav} is set as 3, and d_{cav} as 0.3 m.

This energy balance finds a cavity wall temperature of 1252 K (979 °C) and a cavity efficiency $Q_{g+p,cav}/Q_{in}$ = 56%.

7.2.2. Energy Balance on Reactor Outer Wall

A similar energy balance can be performed on the outer wall of the reactor. Here, the amount of incoming energy from the particle cloud can be balanced with thermal conduction leaving through the insulation. It is assumed that the two walls cannot see each other because of the cloud of particles in between.

The heat entering the wall, $Q_{g+p,w}$ is

$$Q_{g+p,w} = \frac{\pi d_w h_w \epsilon_w \sigma \left(\epsilon_{g+p} T_g^4 - \alpha_{g+p} T_w^4\right)}{\alpha_{g+p} + \epsilon_w - \alpha_{g+p} \epsilon_w}$$

The heat leaving the wall is an energy balance in itself, being made up of two equal fluxes: one through the insulation, and one from the insulation to the air surrounding it.

$$Q_{ins} = \frac{2\pi h_w (T_w - T_{ins}) k_{ins}}{\ln\left(\frac{r_{ins}}{r_w}\right)}$$

$$Q_{conv} = 2\pi r_{ins} h_{env} (T_{ins} - T_{env})$$

It was assumed that the insulation thickness (r_{ins}-r_w) was 5 cm and had a thermal conductivity k_{ins} of 0.3 W/mK. Air was assumed to be flowing past with a heat transfer coefficient h_{env} of 33 W/m^{2}K. This found a temperature of the outside of the insulation T_{ins} of 88 °C and a temperature of the reactor shell T_w of 925 °C (1198 K), slightly below the particles. This meant a heat flux Q_{ins}=Q_{conv}=$Q_{g+p,w}$ of 222 W.

7.2.3. Rate of energy provision for calcination

This heat flux of 222 W away from the particles can be subtracted from the heat flux of 5644 W to the particles, to give a net heat flux of 5422 W that is absorbed by the particle cloud.

To heat up from ambient to 927 °C and calcine, the limestone must absorb approximately 2.6 MJ/kg of energy. At a flow rate of 10 kg/h or 2.8 g/s, this is equivalent to 7475 W, which is more than the net energy input from the cavity. Thus, the low efficiency of the cavity means that the plant cannot run at that flow rate.

There are some caveats to this:

- Cavity design could be altered to reduce the losses; reducing the cavity diameter by 30% increases plant efficiency to 77%, which would theoretically be high enough to provide enough energy for the plant to process 10 kg/h limestone.
- If full integration of the SOCRATCES plant is achieved, preheating from ambient may not be required, depending on the heat losses from the carboniser.
- Full calcination may not be desired; a lower extent may be sufficient for adequate energy storage efficiency. This strategy could improve sorbent lifetime by reducing the extent of sintering.
- The actual temperature of the cavity is likely to be lower, at least in the upper reaches of the calciner, because the particles will be rather cooler than 927 °C. This constant particle temperature was set to simplify the calculations and is a conservative assumption. Lower temperatures in the cavity will reduce the losses, increasing its efficiency.

7.3. Particle flow through the reactor

Particles will enter the top of the reactor and fall freely through the annulus as they heat up. Their speed is a function of the viscosity of the gas and particle size; the residence time is a function of this speed and the length of the reactor.

A calculation for predicting the size of particle aggregates is given in the Annex; this value of n=51 and a terminal velocity of 0.093 m/s is used in this section. This gives a residence time of around 7.5 seconds.

7.3.1. Time period for particles to heat up

For most of this work, the particles have been assumed to absorb heat isothermally at 927 °C. However, they will be cooler than this to begin with. A small dynamic heating program was developed which looked at how quickly the particles would absorb heat from the cavity wall at 980 °C, regardless of particle emission to the cooler outside wall. It would take less than 0.6

seconds for the particles to reach within 1 °C of the wall, which at the terminal velocity given suggests it would have fallen 55 mm in that time.

This program has some simplicities included. Firstly, there is no emission to the far wall. This would actually increase the rate of heating until the particles reached that wall's temperature, but then reduce it at higher temperatures. Secondly, there is no conduction or convection in this model. It can be expected that heat transfer will occur between the particles and the surrounding gas; however, given the conditions in the annulus the gas is likely to be rather close in temperature to the particles.

However, the main simplicity is that calcination is not taken in to account. This is critical for this reactor's design and so should be included in future iterations. The highly endothermic nature of this reaction will suppress the particles' temperature whilst calcination is ongoing, increasing the rate at which the walls pass energy to the cloud. Assuming the particles are at 927 °C, the cavity wall would provide a net radiation flow of 6654 W/m^2. Considering particles falling at terminal velocity, it would take around 21 seconds to provide enough energy for the particles to fully calcine. This suggests that the particles would not fully calcine before they exited the reactor. However, this would have knock-on effects on the temperature of the cavity wall (it would increase) and so slightly more calcination may be achieved within that time period. Another issue is the rate of calcination. At 927 °C, it takes 40 seconds to reach 96% calcination according to the GRPM in Deliverable 3.2. It reaches only 21% after 7.5 seconds. At lower temperatures this extent of calcination reduced somewhat (10% in 7.5 seconds at 915 °C) but equally, if the temperature can be increased to 935 °C, the particles can reach 29% after 7.5 seconds.

Thus, the particles require roughly 21 seconds to absorb all the necessary heat, but only have a residence time of around 7.5 seconds, leading to approximately 30% calcination. This low extent of calcination is due to the characteristics of the reactor; a longer residence time could be achieved with a longer calciner, and therefore a higher extent of calcination achieved. Whilst calcining, it is likely that the particles will stay close to the 'turning temperature' of the limestone, i.e. the equilibrium temperature at 1 atm CO_2, calcining as quickly as energy can be absorbed. This varies slightly between different limestones, but is generally in the 895–910 °C range.

7.4. Modelling using Calix EES Code

As well as the model above, calculations were performed in a version of Calix's EES code for flash calciners. This takes more phenomena in to account. However, the geometry of the reactor is similar to that of the co-current electric calciner and not the solar calciner; i.e. the reaction occurs in the core and the heat is supplied in the annulus. The reactor tube is set to 979 °C, as per the simulation in Excel. However, it is not possible to model the colder outside wall in this case. The extent of reaction after 7.5 seconds can be determined, when the 5 kg/s powder enters at 25 °C with 0.5 kg/s CO_2. The length of the reactor is not of great importance given the other geometrical differences between this model and the solar calciner design.

An important assumption in this model is that the walls' temperatures are not affected by the heat flux through them, something which is not true for the solar calciner. As such, the calciner as modelled in EES requires lots of heat at the beginning (20 kW/m) and much less once the particles are up to temperature, around 2 kW/m, as shown in Figure 16. This would not be easily achievable in a solar calciner, so the temperatures of the reactor tube near the injection point can be reduced to moderate this 'spike'. This is shown in Figure 17.

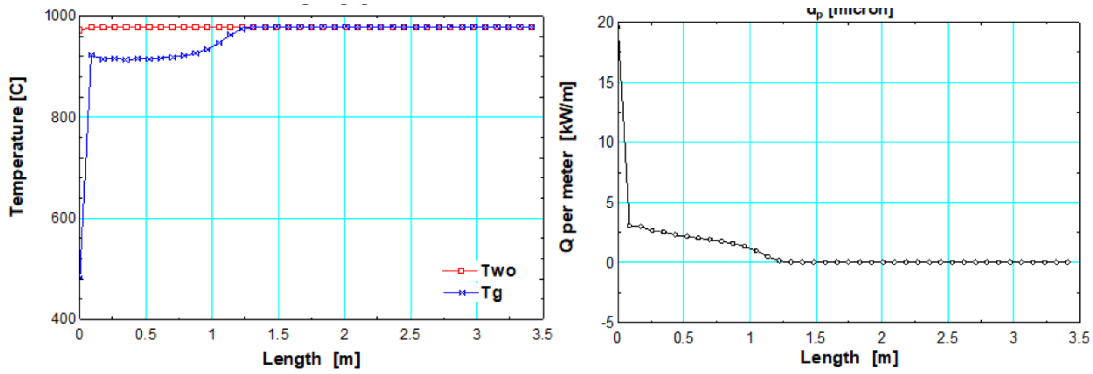

Figure 16: Results from the Calix co-current CFC simulation using GRPM. Wall temperature set at 979 °C throughout (left). Net specific energy flux also shown (right). The residence time was 9.3 seconds.

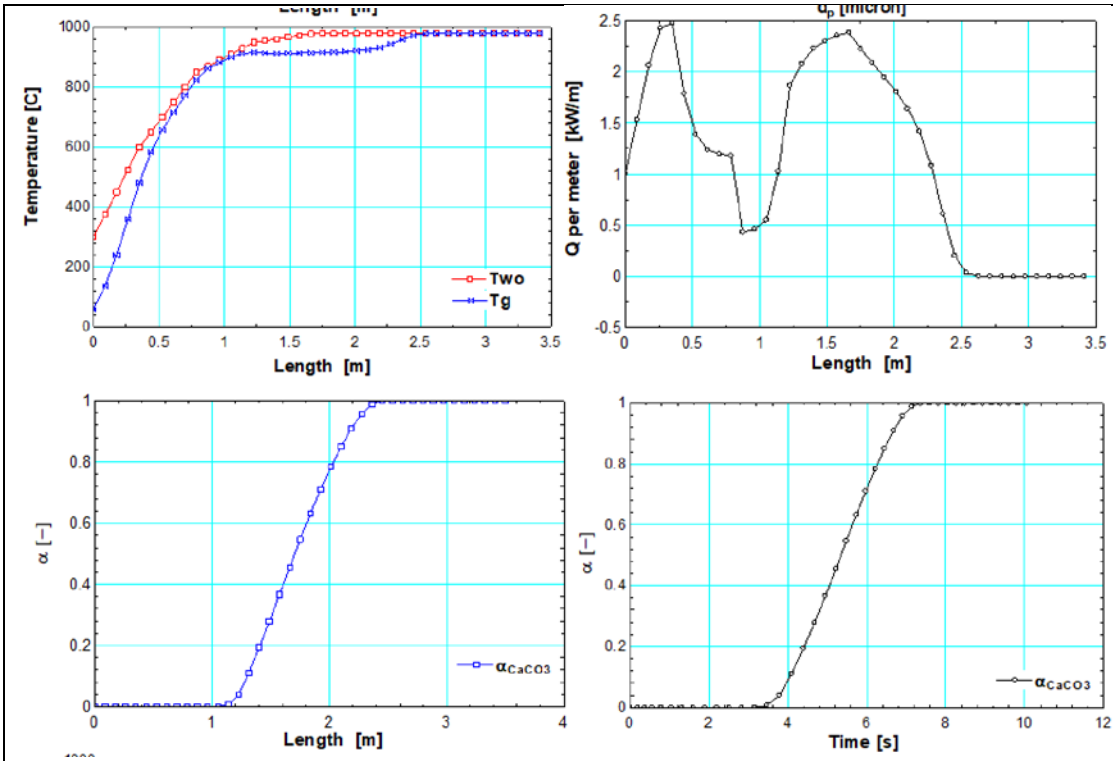

Figure 17: Results from the Calix co-current CFC simulation using GRPM, as shown in the previous Figure but with lower upper wall temperatures, reducing the maximum flux. Note that by 7.5 seconds full calcination has been achieved. Top left: Temperature profile of the wall (red squares) and particle/gas mixture (blue crosses). Top right: Net specific heat flux from wall to particle cloud. Bottom: Extent of calcination as a function of reactor length (left) and residence time (right).

7.5. Role of the Solar Calciner

It is important to keep the role of this calciner in mind. As a proof of concept it should validate the design concept and kinetic modelling. In the case of this solar calciner, high extents of calcination are not necessary as long as the reactor proves its ability to transfer heat from the cavity to the powder. These findings can be extrapolated to larger calciner designs during scale-up which can produce high extents of calcination due to longer residence times and higher solar concentrations.

That said, it may be possible to improve this reactor's performance through some simple modifications. For example, doubling the solar input to 20 kW whilst not altering the aperture

size would increase the efficiency from 56% to 73% and allow a temperature of 1049 °C on the cavity wall instead of 979 °C. This increases the heat flux from the wall to the particles at 927 °C to over 17 kW/m^2 compared with the 6.6 kW/m^2 achievable with 10 kW. Even if the aperture's area had to increase in proportion to the square root of the energy input (r_{ap} = 0.119 m), the efficiency climbs to 63% and the cavity wall temperature is 1035 °C, with the specific wall flux to the particles more than doubling to 14.9 kW/m^2.

8. NEXT STEPS

The solar calciner design is not complete and will rely on close collaboration between WP3 and WP6 to determine what is possible within the constraints of the site, budget and timescale. Issues will arise which require re-design and new calculations to be performed.

The continuation of EES modelling of the solar calciner should continue, with a more rigorous and realistic model being produced. This can help to identify expected performance in a wider range of situations and well as helping to identify any reasons for unexpectedly good or bad performance.

9. SOLAR CALCINER DESIGN & ANALYSIS: CONCLUSIONS

The case for high-temperature, pure-CO_2 atmosphere calcination was put forward as a more compelling concept than low-temperature, low-concentration CO_2 calcination. Whilst this requires compromises with respect to the solar receiver and its efficiency, there are significant benefits, namely: the elimination of gas separation requirements; faster kinetics; and less heat demand within the reactor (since there is a need for only a small amount of gas to be injected).

Several high-temperature designs were proposed. In the end, the indirect flash calciner with a beam-down cavity receiver design was chosen. This has been modelled using two programs from different perspectives to try and understand the design's drawbacks and benefits. Together with the work is Task 3.4 and WP6, the design will continue to be altered to take account of radiative phenomena and challenges regarding construction and operation.

PART THREE: CYLINDRICAL CALCINER MODELLING

The design of the calciner should be validated using a mathematical model which takes geometry, heat transfer and calcination kinetics in to account. In the following, a steady-state mathematical model for calciners has been implemented in EES (Engineering Equation Solver) is presented as the University of Zaragoza's contribution to D3.4.

10. DESCRIPTION

The calciner model is a co-current entrained flow cylindrical reactor. The walls can be maintained at a fixed temperature, or the heat flux across particular lengths of walls can be set. The calciner presents cylindrical geometry with a height of 9 meters, 43 millimetres of internal diameter and 48 mm outside diameter.

The feed flow of stored $CaCO_3$ into the calciner is 5 kg/h or 0,001389 kg/s and the gaseous atmosphere in the calciner is considered to be 100% CO_2. Pressure is considered to be constant along the calciner and equals to 1 bar.

To calculate the residence time of the gas in the calciner, 1D plug flow for the gas is considered. The entraining velocity in downflow for the solid is calculated through the terminal velocity and the gas velocity. The reactor has been discretized in slides of 5 cm length. A summary of the model properties are shown in Table 5.

Table 5. Properties of the calciner model

PARTNER	ZAR	
EQUIPMENT	CALCINER	
SOFTWARE	EES (Engineering Equation Solver)	
SCOPE	Chemical, hydrodynamic and thermal simulations of electrical calciner to assess the design of the equipment and quantification of electric power requirements of the furnaces.	
INPUTS	METHODOLOGY	OUTPUTS
• Inlet conditions of $CaCO_3$ (T_0, P_0, $\dot{m}_{0.CaCO3}$) • Distribution of the power of the furnace ($\dot{q}'_{L_i}$) • Calciner dimensions (L, r_{in}, r_{out}) • Particle diameter (DP)	Two chemical reaction kinetics: • Prout-Tompkins (P-T) kinetic model • Generalised Random Pore (GRP) kinetic model Fluid-dynamics: Solid entraining velocity in downflow (Wen CY., Chaung TZ. Ind. Eng. Chem. Process Des. Dev. Vol. 18 No 4 1979) Heat transfer: VDI Heat Atlas 2010, and 'Emissivity of a cloud of limestone in CO2'	• Flow conditions at length i (T_i, P_i, $\dot{m}_{i.CO2}$, $\dot{m}_{i.CaO}$, $\dot{m}_{i.CaCO3}$) • Conversion and reaction rate at length i (X_i, r_i) • Residence times and velocities of the solid and the gas at length i ($t_{i,s}$, , $t_{i,g}$, $v_{i,s}$, $v_{i,g}$) • Temperature of the calciner at the center, inner wall and outer wall at length i (T_i, $T_{i,iw}$, $T_{i,ow}$) • Required heat for the calcination ($\dot{q}_{i,calc}$) and absorbed heats by convection and radiation at length i ($\dot{q}_i$, $\dot{q}_{i,conv}$, $\dot{q}_{i,rad}$)

11. METHODOLOGY

11.1. Calcination kinetic model

The kinetic model of the calcination under interesting conditions of pressure, temperature and atmosphere were described, along with their derived constants, in Task 3.2 Catalytic Flash Calcination.

In the meanwhile, three calcination kinetic models which may be found in literature have been considered and two of them used to obtain preliminary results of the behaviour of the electric calciner.

11.1.1. Prout-Tompkins calcination kinetic model

The calcination kinetic model developed by Prout & Tompkins is well presented by Valverde [27] and is a sigmoidal function of calcination conversion with a final conversion of 100%. Thus, the calcination reaction is described by Equation 1, which gives the conversion of $CaCO_3$ as a function of time:

$$X(t) = \frac{1}{1 + e^{-r(t-t_0)}} \quad (1)$$

where t_0 is the time taken to reach a 50% conversion of the initial reactant. This value is not provided in the mentioned paper. However, the great dependence of this value on the pressure ratio (P/P_{eq}) may be observed from Figure 22. The lower pressure ratio, the lower t_0. For pressure ratios below 0,7 as those expected to be found in the calciner, this variable value will be the order of several seconds (below 60 s).

The reaction mechanism of calcination considers a first step of chemical decomposition of $CaCO_3$ into a metastable CaO* form and adsorbed CO_2 (R.1) after which the metastable structure transforms into the stable CaO crystal while CO_2 is desorbed (R.2).

1) $CaCO_3$ chemical decomposition.

$$\underset{1-\phi}{\boldsymbol{CaCO_{3\,(s)}} + \boldsymbol{L}} \;\leftrightarrow\; \underset{\phi}{\boldsymbol{CaO^*_{(s)}} + \boldsymbol{LCO_2}} \qquad R.1$$

2) CO_2 desorption / Structural transformation.

$$\underset{\phi}{\boldsymbol{CaO^*_{(s)}} + \boldsymbol{LCO_2}} \;\leftrightarrow\; \underset{P_{CO2}\quad 1-\phi}{\boldsymbol{CaO_{(s)}} + \boldsymbol{CO_{2(g)}} + \boldsymbol{L}} \qquad R.2$$

Since the chemical decomposition stage is the rate-limiting step, the reaction rate of the global reaction is considered to be the reaction rate of R.1. This reaction rate r is given by Equation 2, as a function of temperature and the partial pressure of CO_2:

$$r = k_a \cdot e^{\left(-\frac{E_a}{RT}\right)} \cdot \left(1 - \frac{P_{CO2}}{P_{CO2,eq}}\right) \quad (1-\phi) \quad (2)$$

where k_a is $5 \cdot 10^7$ s^{-1} and E_a is 178 kJ/mol. Besides, the partial pressure of CO_2 under equilibrium is expressed as $P_{CO2,eq} = A \cdot \exp(-\alpha/T)$, where A is $4.083 \cdot 10^7$ atm, and α is 20474 K. Furthermore, the fraction of active sites still empty, $1 - \phi$, may be calculated using Equation 3.

$$1-\phi = \frac{1}{1+e^{-\left(\frac{\Delta G_1{}^0+\Delta G^*}{R\cdot T}\right)}\cdot\left(\frac{P_{CO_2}}{P_{CO_{2,eq}}}\right)} \quad (3)$$

$\Delta G_1{}^0$ and ΔG^* are defined as shown in Equations 4 and 5.

$$\Delta G_1{}^0 = \Delta H_1{}^0 - \Delta S_1{}^0 \cdot T \quad (4)$$

$$\Delta G^* = \Delta H^* - \Delta S^* \cdot T \quad (5)$$

where $\Delta H_1{}^0$ is 208 kJ/mol, $\Delta S_1{}^0$ is 0,0155 kJ/mol-K, ΔH^* is 50 kJ/mol, ΔS^* is 0,086 kJ/mol-K.

AUTH presented the results from their experiments in terms of parameters for calcination kinetic models (GRP and P-T) developed based on their own results for 20% CO2 in N_2 atmosphere. The P-T model has also been implemented in the calciner model. The evolution of the conversion will follow the same expression provided in Equation 1 where t_0 takes values between 4.42 and 10.10s as seen in the figures shown during the mentioned SOCRATCES WP3 meeting for 900, 925 and 950 °C. In this version of the P-T kinetic model, the calcination reaction rate is as given by Equation 6.

$$r = k_o \cdot e^{\left(-\frac{E_a}{RT}\right)} \cdot \left(1-\frac{P_{CO2}}{P_{CO2,eq}}\right) \cdot \left(\frac{1}{1+\left(\frac{P_{CO2}}{P_{CO2,eq}}\right)\cdot e^{\left(\frac{\Delta S_1^o}{R}\right)}\cdot e^{\left(-\frac{\Delta H_1^o}{RT}\right)}}\right) \quad (6)$$

where k_o is 4,69·10^9 s^{-1} and E_a is 230 kJ/mol. The values of ΔS_1^o and ΔH_1^o were respectively taken as 0.068 kJ/kmol-K and 160 kJ/mol as provided by AUTH in the Table 4 of D3.2 SOCRATCES calciner kinetics model from Ortiz et al. [28].

11.1.2. GRP calcination kinetic model

AUTH presented their calcination kinetic models' constants developed based on their own experimental results for 900, 925 and 950 °C. The P-T model has also been implemented in the calciner model. The evolution of the conversion, $\alpha(t)$, with the residence time of the solid will follow the expression provided in Equation 7.

$$\alpha(t) = \int_0^t k\frac{6\cdot\left(d_p 2kt\right)^2}{d_p^3}dt + \left(1-e^{\left(-S_{A0}kt-\pi L_{A0}(kt)^2\right)}\right)\int_t^{d_p/2k} k\frac{6\cdot\left(d_p 2kt\right)^2}{d_p^3}dt \quad (7)$$

where S_{A0} is the pore surface area calculated as the difference between BET surface area (1108700 m^2/m^3) and geometrical surface area and L_{A0} is the mean pore length with a value of 4.39E+12 m/m^3. A mean particle diameter of 60 microns was used.

In the GRP kinetic model, the calcination reaction rate, k [m/s], is the fitting parameter of conversion calculation through the Equation 7 to the experimental data. The reaction rate is given by Equation 8 when the atmosphere in the calciner is pure CO_2.

$$k = k_o \cdot e^{\left(-\frac{E_a}{RT}\right)} \cdot (1-\theta_{CO2})^{N_v} \cdot \left(1-\frac{P_{CO2}}{P_{CO2,eq}}\right) \quad (8)$$

where $k_o$takes the value of 0.021 m/s, E_a is 130 kJ/mol, N_v is considered to take the value of 1 and θ_{CO2} is defined through Equation 9.

$$\theta_{CO2} = \frac{\frac{P_{CO2}}{P_{CO2,eq}}}{\left(1+\frac{P_{CO2}}{P_{CO2,eq}}\right)} \quad (9)$$

The kinetic models allow for computing the conversion of each component as a function of time. Therefore, to characterize the mass flows of different components, it is required to know the temperature, the residence time of solid and the gas in the reactor.

The PT and GRP calcination kinetic models, together with their constants developed by AUTH have been implemented in the EES overall model of electric calciner whose results are presented in this report.

11.2. Residence time for the solids

The time of interaction between the solid and the gas is limited to the residence time of the solid in the calciner since its terminal velocity must be also accounted. For those flows with Reynolds lower than 2 and small size particles, the following Equation 10 may be applied for the downward velocity of single particles, v_s, (concentration of particles is assumed diluted) [29]:

$$v_s = v_{s,i} \cdot e^{-bt_s} + \left(v_g + v_t\right) \cdot \left(1 - e^{-bt_s}\right) \tag{10}$$

where $v_{s,i}$ is the initial velocity of the solid, v_g is the velocity of the gas phase, and v_t is the terminal settling velocity of the particle in a static fluid. The parameter b, and the velocity v_t are given by Equation 11 and Equation 12:

$$b = \frac{18\mu}{\rho_s d_p^2} \tag{11}$$

$$v_t = \frac{\left(\rho_s + \rho_g\right) d_p^2 g}{18\mu} \tag{12}$$

where μ is the viscosity of the gas, ρ_s is the density of the solid, ρ_g is the density of the gas, d_p is the diameter of the solid particles, and g the gravity.

The integration of Equation 10 provides the relationship between the calciner length and the residence time of the solids (Equation 13).

$$L = \int_0^{t_{s,L}} v_s dt_s = \frac{v_{s,i}}{b}\left(1 - e^{-bt_s}\right) + \left(v_g + v_t\right) \cdot \left(t_s - \frac{1 - e^{-bt_s}}{b}\right) \tag{13}$$

It can be assumed that v_g and μ are constants in the interval of integration for the case of study. Moreover, the variation of v_t with time (due to the variation of ρ_g) can also be neglected when integrating, since $v_g \gg v_t$.

Thus, this can be directly solved by the EES software to compute the residence time of the solid as a function of the length, what will allow determining the mole flows along the reactor as a function of the distance from the entrance.

11.3. Plug flow model (1D) for the gas

The residence time of the gas is given by Equation (14):

$$t_g = \int_0^{V_c} \frac{\pi r_{in}^2}{\dot{V}} dL \tag{14}$$

where r_{in} is the inner radius of the calciner, $\dot{V}$ is the volumetric flow rate, and V_c the calciner volume. Moreover, $\dot{V}$ is the product of the gas velocity multiplied by the cross-sectional area of the reactor, which in the study case must be corrected by subtracting the area occupied by the solid. The variation in the effective cross-sectional area along the reactor may be neglected as $CaCO_3$ is consumed when CaO is produced.

Besides, it is assumed that the pressure inside the reactor remains constant. Hence, the volumetric flow rate is given by Equation 15, according to the ideal gas law:

$$\dot{V}_{L2} = \frac{(1 + X_{L2}) \cdot T_{L2}}{T_{L1}} \dot{V}_{L1} \tag{15}$$

The residence time of the gas, through a length L_i in which $\dot{V}_{Li}$ can be considered constant will be $t_{g(L1)} = L_i \cdot S_{eff}/\dot{V}_{Li}$.

11.4. Heat transfer model

The following steps are taken to compute the heat transfer to the cloud of gas and particles to the cooling fluid. First, an energy balance inside the reactor is computed for each slice of reactor (from length L_{i-1} to length L_i) by Equation 16:

$$\sum_{\substack{j=CaO,\\ CO2,\\ CaCO3}} Cp_j \cdot \dot{n}_{j,L_i} \cdot \left(T_{L_i} - T_{L_{i-1}}\right) = \Delta H_r \cdot \left(\dot{n}_{CaCO3,L_i} - \dot{n}_{CaCO3,L_{i-1}}\right) + \dot{q}'_{L_i} \cdot (L_i - L_{i-1}) \tag{16}$$

where Cp_j and $\dot{n}_j$, are the specific heat and mole flow of component j, respectively, T is the temperature of the cloud of gas and particles (which is assumed homogeneous inside the carbonator), ΔH_r is the heat of reaction (178 kJ/mol), and $\dot{q}'_{L_i}$ is the heat flow throughout the inside wall of the carbonator per unit of length. The latter accounts for radiation and convection, in the form of Equation 17:

$$\dot{q}'_{L_i} = \dot{q}'_{rad,L_i} + \dot{q}'_{conv,L_i} \tag{17}$$

$$\dot{q}'_{rad,L_i} = \frac{\varepsilon_w}{\alpha_{g+p} + \varepsilon_w - \alpha_{g+p} \cdot \varepsilon_w} \cdot \sigma \cdot (\varepsilon_{g+p} \cdot T^4_{iw,L_i} - \alpha_{g+p} \cdot T^4_{L_i}) \cdot 2\pi r \tag{18}$$

$$\dot{q}'_{conv,L_i} = h_{g,L_i} \cdot \left(T_{iw,L_i} - T_{L_i}\right) \cdot 2\pi r \tag{19}$$

Where α_{g+p} and ε_{g+p} are the absorptivity and emissivity of the gas-particle mixture, ε_w the emissivity of the carbonator wall, σ is the Boltzmann's constant, T_{iw} is the temperature of the inner wall of the carbonator, r the inner radius of the carbonator, and h_g the convective coefficient.

The model for the calculation of the absorptivity and emissivity of the gas-particle mixture is borne out of 'Heat Transfer' by Nellis and Klein [30], and follows Equations 20 to 24:

$$h_{g,L_i} = \frac{Nu_{Li} \cdot k_{Li}}{2r} \tag{20}$$

$$Nu_{L_i} = 3.66 + \frac{\left(0.049 + \frac{0.020}{Pr_{Li}}\right) \cdot Gz_{Li}^{1.12}}{1 + 0.065 \cdot Gz_{Li}^{0.7}} \tag{21}$$

$$Pr_{Li} = \frac{Cp_{Li} \cdot \mu_{Li}}{k_{Li}} \tag{22}$$

$$Gz_{Li} = \frac{Re_{Li} \cdot Pr_{Li}}{L/2r} \tag{23}$$

$$Re_{Li} = \frac{4 \cdot \dot{m}_{Li}}{\pi \cdot 2r \cdot \mu_{Li}} \tag{24}$$

Where Nu is the Nusselt number, k the thermal conductivity, Pr the Prandtl number, Gz the Graetz number, μ the viscosity, Re the Reynolds number, and $\dot{m}$ the mass flow.

The temperature of the outer wall of the calciner, T_{ow}, is computed by the formula of heat conduction through a tube wall, given by Equation 25:

$$\dot{q}'_{L_i} = \frac{T_{0w,L_i} - T_{iw,L_i}}{R_{tube} \cdot L_i} \quad (25)$$

$$R_{tube} = \frac{\ln(\frac{r_{out}}{r})}{2\pi \cdot k_{tube} \cdot L_i} \quad (26)$$

where R_{tube} is the thermal resistance of the carbonator tube, r_{out} the outer radius of the calciner, and k_{tube} the thermal conductivity of the calciner tube (0.025 kW/m·K).

12. RESULTS

12.1. Isothermal operation

The calciner is 9-meter-long, 43 mm in diameter, and 5 mm in thickness. The cases presented initially implement two different calcination kinetic models (i) the Prout-Tompkins model and (ii) the Generalised Random Pore kinetic model. The demand of heat per length unit required to maintain constant temperature in the calciner has also been calculated in the simulations. These values will be later used to define the heat flow pattern introduced along the calciner and the power and number of independent segments.

12.1.1. P-T calcination kinetic model

The following cases implement the Prout-Tompkins calcination kinetic model and consider isothermal operation. It is important to notice that EES simulations have been run under 100% CO_2 atmosphere while the P-T model has been adjusted using experimental data obtained under 20% CO_2 in N_2 atmosphere. The cases initially presented implement the calcination kinetic model and consider isothermal operation. The required input of heat per length unit to maintain constant temperature has also been calculated.

The residence time of the particles ranges between 28-30 seconds (particle diameter of 60 μm) depending on the temperature (975 °C–925 °C) and the corresponding conversion of limestone. The higher conversion, the higher production of CO_2 and the higher velocity of the gas and solid cloud inside the calciner.

The pressure inside the calciner is assumed 1.0 bar (pure CO_2 atmosphere) and the simulated temperatures varies from 925 °C to 975 °C. The initial mass flow of $CaCO_3$ is 5 kg/h. Results obtained for 900 °C are not presented in Figure 19 given the low conversion achieved and the strong deviation from reality (conversion equals to zero at the initial moment) of calculated conversion at zero seconds.

This deviation in the estimation of limestone conversion at the initial moment leads to an extremely high overestimation of the heat required for calcination in the very first part of the calciner which is also observed for higher temperatures although cushioned. Therefore, the use of P-T kinetic model may be not recommended when an accurate distribution of heat supply along the calciner has to be defined.

The conversion profiles of the calciner are presented in Figure 19 together with solid time residence and required heat flow per unit length. The final conversion varies from 97.89% to 100% for 925 °C and 975 °C respectively. If temperature is kept between 950–975 °C, total conversion is ensured in the calciner outlet under the simulated conditions (100% CO_2).

The calcination reaction rates are increased with the temperature of the reactor from 0.1597 s^{-1} to 0.7537 s^{-1}. The pressure ratio between the partial pressure of CO_2 and the pressure of equilibrium of CO_2 varies from 0.6376 for the most disadvantaged simulated situation (925 °C) to 0.3215 for the most advantaged situation (highest simulated temperature, 975 °C).

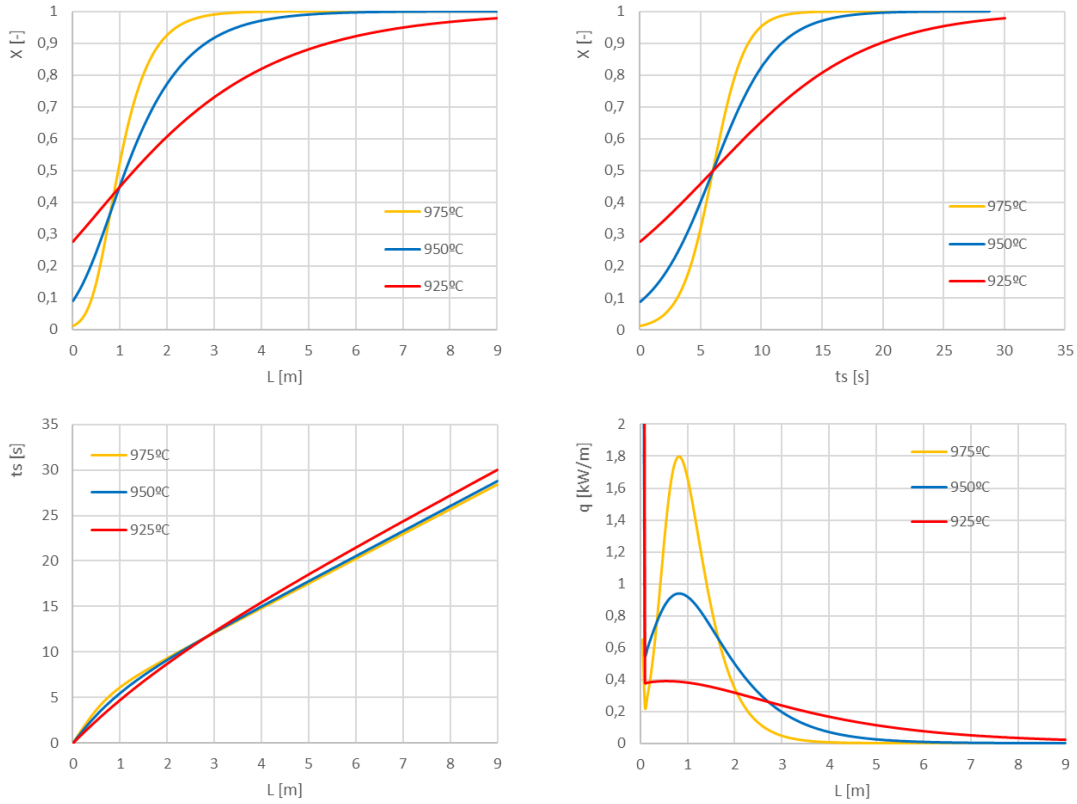

Figure 18. P-T at 1 bar – 100% CO_2. (Top left) Conversion profiles of the calciner (X) vs. length, (Top right) conversion vs. solid residence time, (Bottom left) solids residence time (ts) vs. calciner length and (Bottom right) required heat per unit length (q) vs. length

12.1.2. GRP calcination kinetic model

The following cases implement the GRP calcination kinetic model developed by Calix with parameters calculated by AUTH and consider isothermal operation. It is important to notice that EES simulations have been run under 100% CO_2 atmosphere while GRP model has been adjusted using experimental data obtained under 20% CO_2 in N_2 atmosphere. The cases initially presented implement the calcination kinetic model presented in D3.2 and consider isothermal operation. The required input of heat per length unit to maintain constant temperature has also been calculated.

The residence time of the particles ranges between 28–63 seconds (particle diameter of 60 µm) depending on the temperature (975 °C–900 °C) and the corresponding conversion of limestone. The higher conversion, the higher production of CO_2 and the higher velocity of the gas and solid cloud inside the calciner. The equilibrium temperature for a 100% CO_2 atmosphere and atmospheric pressure is approx. 895 °C.

The pressure inside the calciner is assumed 1.0 bar (pure CO_2 atmosphere) and the simulated temperatures varies from 900 °C to 975 °C. The initial mass flow of $CaCO_3$ is 5 kg/h. The GRP kinetic model provides a more accurate value of conversion profile along the calciner. This accuracy makes it more suitable to realistically define the required heat distribution along the calciner.

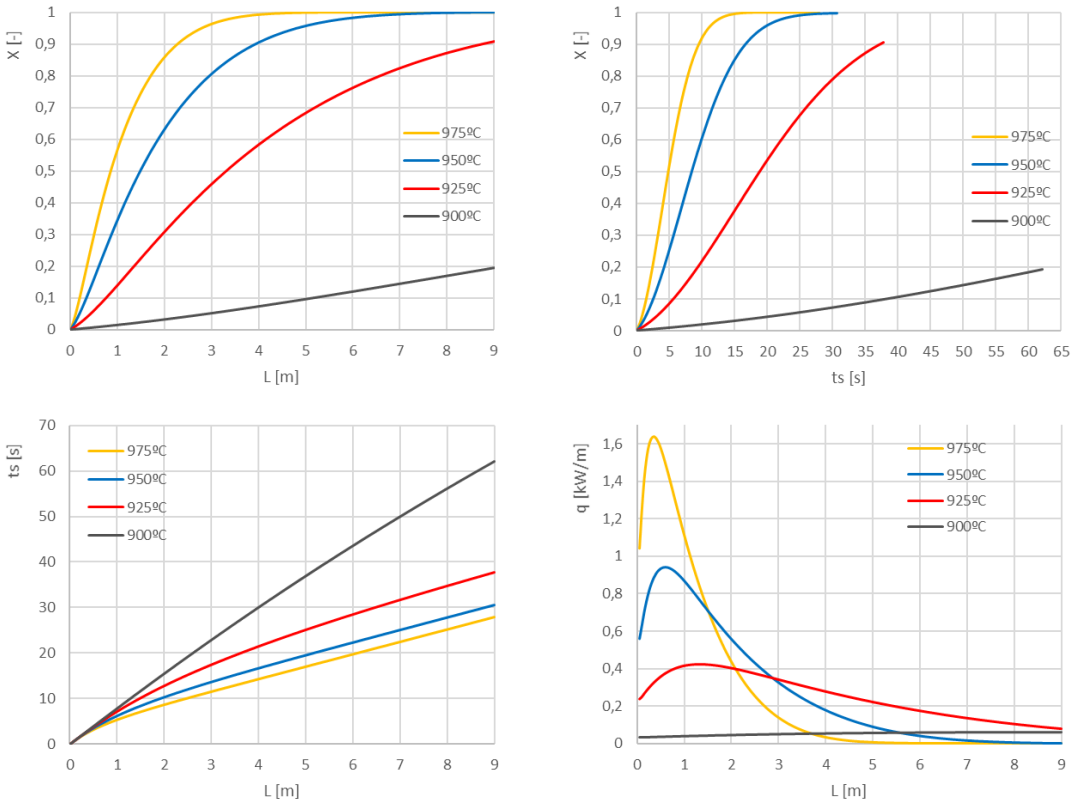

Figure 19. GRP at 1bar – 100% CO_2. (Top left) Conversion profiles of the calciner (X) vs. length, (Top right) conversion vs. solid residence time, (Bottom left) solids residence time (ts) vs. calciner length and (Bottom right) required heat per unit length (q) vs. length.

The conversion profiles of the calciner are presented in Figure 20 together with solid time residence and required heat flow per unit length. The final conversion varies from 20% to 100% for 900 °C and 950-975 °C respectively. If temperature is kept between 950–975 °C, total conversion is ensured in the calciner outlet under the simulated conditions (100% CO_2).

12.2. Constant heat flow

In this section, a constant heat flow is supplied to the calciner over segments of the calciner wall and the effect on temperature profile and conversion is calculated. The initial mass flow of $CaCO_3$ is considered 5 kg/h.

Several configurations of segments are simulated to check the influence of heat power distribution, number of independent segments and length of such segments. The objective is to achieve flat profiles of temperature along the calciner with temperatures around 975–985 °C to promote limestone conversion preventing particle sintering. As seen in the following subsection, different heat flow profiles are required depending on the implemented kinetic model. Initially, results obtained implementing the P-T kinetic model are shown. Then, results obtained applying the GRP kinetic model are presented.

12.2.1. P-T calcination kinetic model

The first case study considers an inlet temperature of the $CaCO_3$ from the solar calciner of 975 °C. The electric power of the furnaces which have been simulated are distributed in eight units (*Profile 1*): (i) 0.5 m 120W/m, (ii) 0.5 m 900 W/m, (iii) 1 m 1200 W/m, (iv) 1 m 400 W/m, (v) 1 m 100 W/m, (vi) 1 m 20 W/m, (vii) 1 m 8 W/m, (viii) 1 m 2 W/m (ix) 2 m without electric furnace. This distribution and the temperature profile along the calciner are shown in Figure 21 (Left).

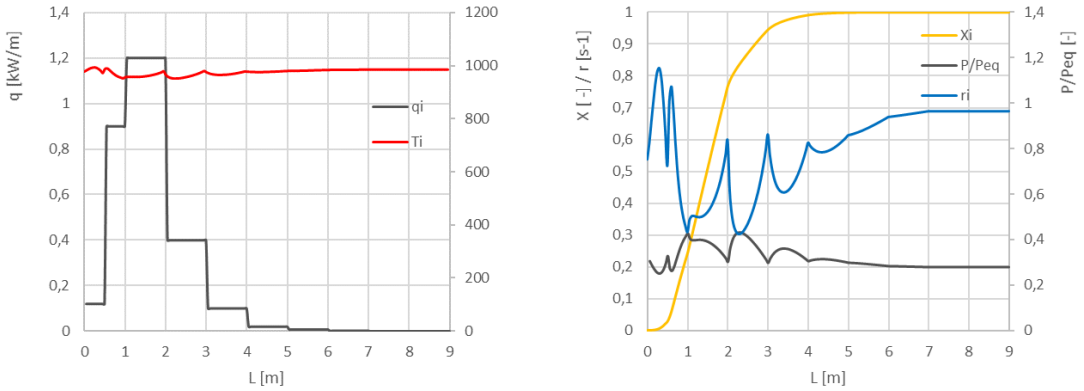

Figure 20. P-T at 1 bar – 100% CO_2. (Left) Supplied heat per unit length (q) and temperature (T) vs. calciner length and (Right) Conversion profile of the calciner (X), reaction rate (r) and partial pressure ratio (P/Peq) vs. calciner length.

A second case considers again an inlet temperature of the $CaCO_3$ from the solar calciner of 975 °C (lower temperatures at the entrance will lead to incoherent results from the P-T kinetic EES model given the higher initial conversion for lower temperatures). The power distributions are (*Profile 2*): (i) 0.5m 40 W/m. (ii) 0.5 m 400 W/m (iii) 1 m 1500 Wm, (iv) 0.5 m 600 W/m, (v) 1 m 150 W/m, (vi) 1.5 m 20 W/m and (vii) no heating is modelled in the last four meter of the calciner.

The comparison between both temperature and conversion profiles are shown in Figure 21. Both heat supply profiles lead to a 100% limestone calcination under 20 seconds which corresponds to approximately the first four meters of the calciner. Depending on the heat supply and the corresponding temperature within the calciner, the reaction rate is increased or decreased as seen in Figure 22.

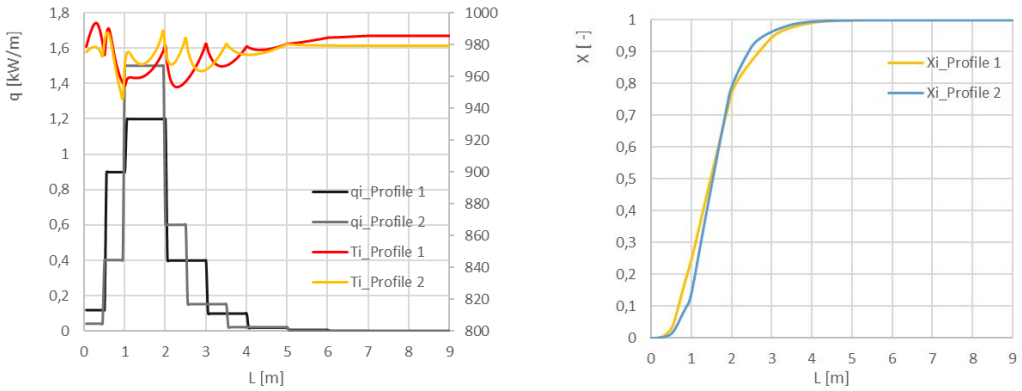

Figure 21. PT at 1 bar – 100%CO_2. (a) Supplied heat per unit length (q) and temperature (T) vs. calciner length and (b) Conversion profile of the calciner (X) vs. calciner length.

12.2.2. GRP calcination kinetic model

This case study considers an inlet temperature of the $CaCO_3$ from the solar calciner of 895 °C. The power of the segments which have been simulated are distributed in four units (*Profile 3*): (i) 2 m 800 W/m, (ii) 1 m 500 W/m, (iii) 1 m 300 W/m, (iv) 2 m 80 W/m, (v) 3 m without electric furnace. This distribution and the temperature profile along the calciner are shown in Figure 23 (Left).

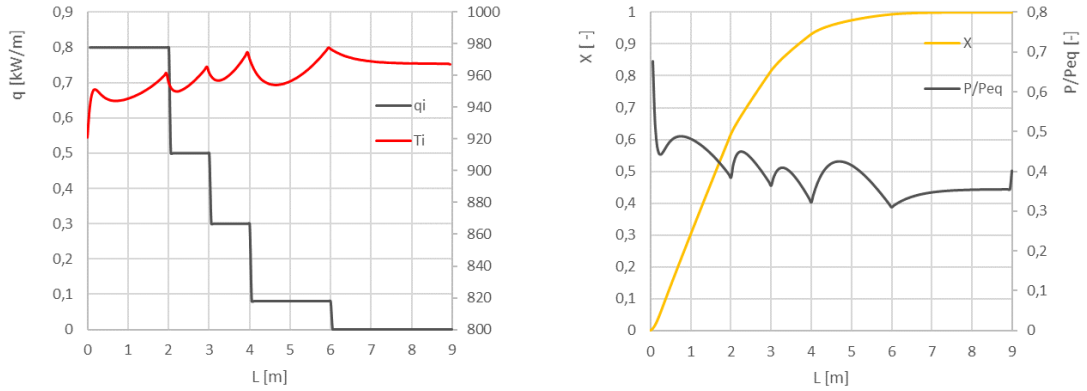

Figure 22. GRPM at 1 bar – 100%CO_2. (Left) Supplied heat per unit length (q) and temperature (T) vs. calciner length and (Right) Conversion profile of the calciner (X) vs. calciner length.

This heat supply distribution achieves 99% calcination of limestone after approximately 25 seconds (6.5 meters) without extreme temperature peaks and a flat temperature profile around 960 °C (average temperature 960.1 °C). The total need of power is 2560 W along the whole reactor.

The next proposal of heat distribution pretends to reduce the power demand while operating at the lowest possible temperature and achieving total calcination. This case study considers an inlet temperature of the $CaCO_3$ from the solar calciner of 895 °C. The power of the furnaces which have been simulated are distributed in six units (*Profile 4*): (i) 1 m 500 W/m, (ii) 1 m 1000 W/m, (iii) 1 m 500 W/m, (iv) 1 m 300 W/m, (v) 2 m 80 W/m, (vi) 1 m 50 W/m, (vii) 2 m without furnace. This distribution and the temperature profile along the calciner are shown in Figure 24 (Left).

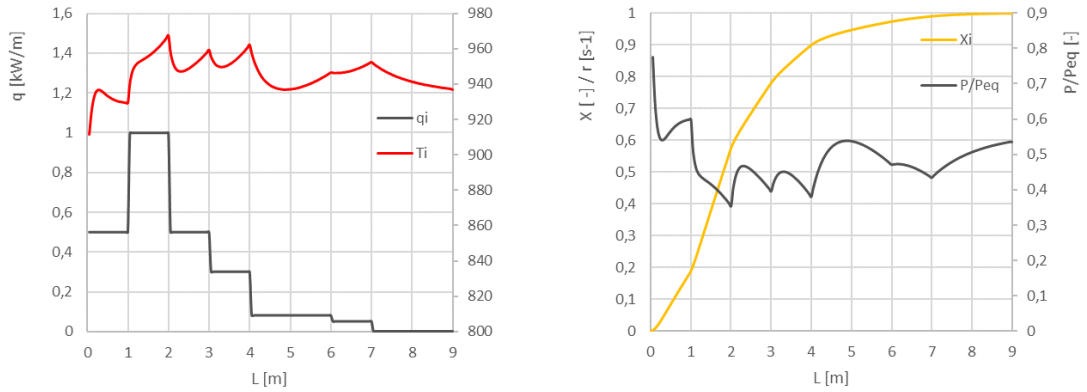

Figure 23. GRPM at 1 bar – 100%CO_2. (Left) Supplied heat per unit length (q) and temperature (T) vs. calciner length and (Right) Conversion profile of the calciner (X) vs. calciner length.

This heat supply distribution achieves the total calcination of limestone (7.5 meters) without temperature peaks and a flat temperature profile around 950 °C (average temperature 945 °C). The total need of power is 2510 W along the whole reactor. Figure 25 presents the comparison between both profiles, Profiles 3 and 4, and shows total calcination for both scenarios. Heat supply and temperatures are somehow lower for Profile 4 and the consequent slower calcination reaction is illustrated in Figure 25 (Right).

It is worth to remind that for lower inlet temperatures of limestone the heat profiles will be strongly modified. Therefore, further simulations where inlet limestone temperature ranges between 25–400 °C will also be assessed.

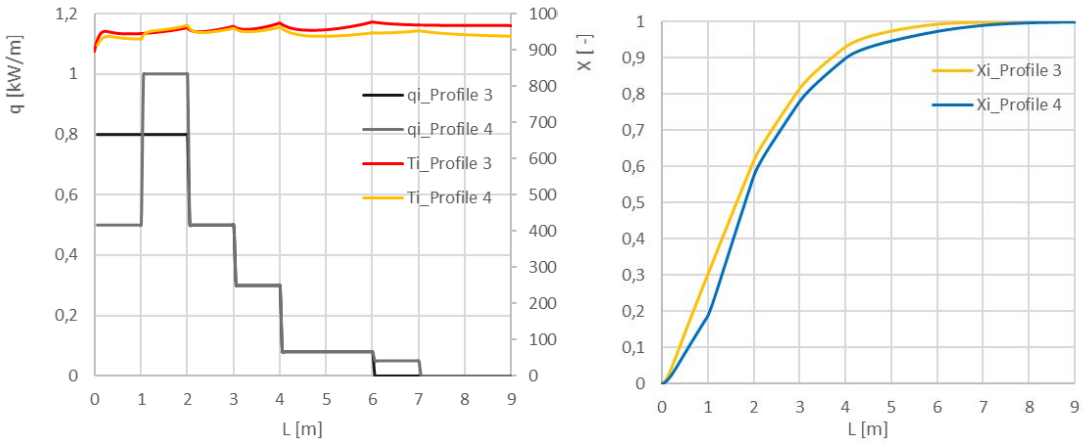

Figure 24. GRPM at 1 bar – 100%CO_2. (Left) Supplied heat per unit length (q) and temperature (T) vs. calciner length and (Right) Conversion profile of the calciner (X) vs. calciner length.

13. CYLINDRICAL CALCINER MODELLING: CONCLUSIONS

The use of P-T kinetic model may be not recommended when an accurate distribution of heat supply along the calciner has to be defined. It leads to an important overestimation of calcination conversion for initial condition (t=0) which introduces a strong distortion of heat requirement profiles. Therefore, GRP model will be the kinetic model used to provide further simulations on the behaviour of calciners.

Results obtained for isothermal cases (using both kinetic models) revealed that temperature between 950–975 °C ensure total conversion at the calciner outlet under simulated conditions (atmospheric pressure and 100% CO_2).

Different heat supply profiles have been implemented and all of them allow to achieve total calcination of 5 kg of limestone per second inside the electric calciner. Depending on the kinetic model considered and the heat profiles, total calcination is achieved between 4.5 and 7.5 meters. The residence time of solids required to achieve 99% of calcination ranges between 20-30 seconds.

A proper control of power of the furnaces avoids extreme temperature peaks along the calciner. A relatively flat temperature profile around 950–960 °C was achieved in the reactor. The total power requirement when limestone is introduced at high temperature (considering that it comes from the previous solar calciner at 895 °C) is around 2500 W mostly concentrated along the first four meters of the reactor.

These findings are key results for the calciner and auxiliary heater designs. The cylindrical model represents what is desired for the reaction side of the auxiliary heater, and thus it could be extended to include modelling of the outer wall of the reactor and the electric elements which are expected to surround it. There is also potential to alter the cylindrical geometry to reflect the indirect solar CFC's design. Integrating the solar receiver results with it to develop a more sophisticated model of the solar calciner than was presented in Part Two would provide a powerful tool. Regardless, the modelling here provides a basis for future investigations of all calciner designs.

14. REFERENCES

[1] W. Mak, A. Heimisson, P. Borondo, L. Robins, and U. Schnyder, "Delivering 'Net Zero' - Will the wholesale market cease to function in a high renewables world?," 2018.

[2] T. P. Hills, M. Sceats, D. Rennie, and P. Fennell, "LEILAC: Low Cost CO2 Capture for the Cement and Lime Industries," in *Energy Procedia*, 2017, vol. 114, pp. 6166–6170.

[3] "Calix | Agriculture, Wastewater, Infrastructure Solutions & More." [Online]. Available: https://www.calix.com.au/. [Accessed: 31-Aug-2018].

[4] A. Castellanos, J. M. Valverde, and M. A. S. Quintanilla, "Aggregation and sedimentation in gas-fluidized beds of cohesive powders," *Phys. Rev. E*, vol. 64, no. 4, p. 041304, Sep. 2001.

[5] E. Lemmon, M. McLinden, and D. Friend, "Thermophysical Properties of Fluid Systems," Gaithersburg, Maryland, USA, 2018.

[6] J. Blamey, E. J. J. Anthony, J. Wang, and P. S. S. Fennell, "The calcium looping cycle for large-scale CO2 capture," *Prog. Energy Combust. Sci.*, vol. 36, no. 2, pp. 260–279, Apr. 2010.

[7] I. Barin, *Thermochemical data of pure substances*, 3rd ed. Wiley Interscience, 2008.

[8] C. A. Scholes and U. K. Ghosh, "Review of Membranes for Helium Separation and Purification.," *Membranes (Basel).*, vol. 7, no. 1, Feb. 2017.

[9] P. Häussinger *et al.*, "Noble Gases," in *Ullmann's Encyclopedia of Industrial Chemistry*, Weinheim, Germany: Wiley-VCH Verlag GmbH & Co. KGaA, 2001.

[10] N. Casas, J. Schell, R. Blom, and M. Mazzotti, "MOF and UiO-67/MCM-41 adsorbents for pre-combustion CO2capture by PSA: Breakthrough experiments and process design," *Sep. Purif. Technol.*, vol. 112, pp. 34–48, Jul. 2013.

[11] C. Branan, *Rules of Thumb for Chemical Engineers*, Fourth Edi. Burlington, MA: Elsevier, 2005.

[12] H. P. Loh, J. Lyons, and C. W. I. White, "Process Equipment Cost Estimation - Final Report," 2002.

[13] "Plant Cost Index - Chemical Engineering." .

[14] "CEPCI Updates: January 2018 (prelim.) and December 2017 (final) - Chemical Engineering," *Chemical Engineering Online*, 2018. [Online]. Available: https://www.chemengonline.com/cepci-updates-january-2018-prelim-and-december-2017-final/?printmode=1. [Accessed: 10-Dec-2018].

[15] Eurostat, "Natural gas prices for non-household consumers," *Natural Gas Price Statistics*, 2018. [Online]. Available: https://ec.europa.eu/eurostat/statistics-explained/index.php/Natural_gas_price_statistics#Natural_gas_prices_for_non-household_consumers. [Accessed: 10-Dec-2018].

[16] J. M. Valverde, P. E. Sanchez-Jimenez, and L. A. Perez-Maqueda, "Limestone calcination nearby equilibrium: Kinetics, CaO crystal structure, sintering and reactivity," *J. Phys. Chem. C*, vol. 119, no. 4, pp. 1623–1641, 2015.

[17] J. M. Criado, M. Gonzalez, J. Malek, A. Ortega, M. Gonzfilez, and A. Ortega, "The effect of the CO2 pressure on the thermal decomposition kinetics of calcium carbonate," *Thermochim. Acta*, vol. 254, no. 121, pp. 121–127, Apr. 1995.

[18] Z. Liao and A. Faghri, "Thermal analysis of a heat pipe solar central receiver for concentrated solar power tower," *Appl. Therm. Eng.*, vol. 102, pp. 952–960, Jun. 2016.

[19] Daniels Fans, "High Temperature Fan | Daniels Fans." [Online]. Available: https://www.danielsfans.com/high-temperature-fans/. [Accessed: 16-Nov-2018].

[20] D. Moore, "Enthalpy of Raw Minerals," *Cement Plants and Kilns in Britain and Ireland*, 2017. [Online]. Available: https://cementkilns.co.uk/cemkilndoc019.html. [Accessed: 28-Nov-2018].

[21] Y. S. Touloukian and D. P. DeWitt, "Thermophysical Properties of Matter: The TPRC Data Series, Volume 7: Thermal Radiative Properties - Metallic Elements and Alloys," West

Lafayette, USA, 1970.
[22] A. Imhof, “The cyclone reactor - an atmospheric open solar reactor,” *Sol. Energy Mater.*, vol. 24, no. 1–4, pp. 733–741, Dec. 1991.
[23] C. K. Ho, S. S. Khalsa, and N. P. Siegel, “Modeling On-Sun Tests of a Prototype Solid Particle Receiver for Concentrating Solar Power Processes and Storage,” in *ASME 2009 3rd International Conference on Energy Sustainability, Volume 2*, 2009, pp. 543–550.
[24] T. Kodama *et al.*, “Particles fluidized bed receiver/reactor tests with quartz sand particles using a 100-kWth beam-down solar concentrating system at Miyazaki,” in *AIP Conference Proceedings*, 2017, vol. 1850, no. 1, p. 100012.
[25] G. Flamant, D. Gauthier, C. Boudhari, and Y. Flitris, “A 50 kW Fluidized Bed High Temperature Solar Receiver: Heat Transfer Analysis,” *J. Sol. Energy Eng.*, vol. 110, no. 4, p. 313, Nov. 1988.
[26] M. I. Roldán Serrano, “Heat Transfer Fluids Used in Concentrating Solar Thermal Technologies,” in *ModellingConcentrating Solar Thermal Technologies: Analysis and Optimisation by CFD*, Springer, Cham, 2017, pp. 73–85.
[27] J. M. Valverde, “On the negative activation energy for limestone calcination at high temperatures nearby equilibrium,” *Chem. Eng. Sci.*, vol. 132, pp. 169–177, 2015.
[28] C. Ortiz, J. M. Valverde, R. Chacartegui, and L. A. Perez-Maqueda, “Carbonation of Limestone Derived CaO for Thermochemical Energy Storage: From Kinetics to Process Integration in Concentrating Solar Plants,” *ACS Sustain. Chem. Eng.*, vol. 6, no. 5, pp. 6404–6417, May 2018.
[29] C. Y. Wen and T. Z. Chaung, “Entrainment Coal Gasification Modeling,” *Ind. Eng. Chem. Process Des. Dev.*, vol. 18, no. 4, pp. 684–695, 1979.
[30] G. Nellis and S. Klein, *Heat transfer*. Cambridge University Press, 2008.
[31] S. Kabelac and D. Vortmeyer, “VDI Heat Atlas Part K - Radiation,” in *VDI Heat Atlas*, Second., VDI, Ed. Springer-Verlag Berlin Heidelberg, 2010.
[32] A. Steinfeld, A. Imhof, and D. Mischler, “Experimental Investigation of an Atmospheric-Open Cyclone Solar Reactor for Solid-Gas Thermochemical Reactions,” *J. Sol. Energy Eng.*, vol. 114, no. 3, pp. 171–174, Aug. 1992.
[33] W. Durisch, “Some physical and chemical experiments under concentrated solar radiation and some thermodynamic considerations,” *Sol. Energy Mater.*, vol. 24, no. 1–4, pp. 508–521, Dec. 1991.
[34] A. Imhof, “Decomposition of limestone in a solar reactor,” *Renew. Energy*, vol. 10, no. 2–3, pp. 239–246, Feb. 1997.
[35] A. Steinfeld, M. Brack, A. Meier, A. Weidenkaff, and D. Wuillemin, “A solar chemical reactor for co-production of zinc and synthesis gas,” *Energy*, vol. 23, no. 10, pp. 803–814, Oct. 1998.
[36] A. Meier, E. Bonaldi, G. M. Cella, W. Lipinski, D. Wuillemin, and R. Palumbo, “Design and experimental investigation of a horizontal rotary reactor for the solar thermal production of lime,” *Energy*, vol. 29, no. 5–6, pp. 811–821, Apr. 2004.
[37] A. Meier, E. Bonaldi, G. M. Cella, and W. Lipinski, “Multitube Rotary Kiln for the Industrial Solar Production of Lime,” *J. Sol. Energy Eng.*, vol. 127, no. 3, p. 386, Aug. 2005.
[38] A. Z’Graggen, P. Haueter, D. Trommer, M. Romero, J. C. de Jesus, and A. Steinfeld, “Hydrogen production by steam-gasification of petroleum coke using concentrated solar power—II Reactor design, testing, and modeling,” *Int. J. Hydrogen Energy*, vol. 31, no. 6, pp. 797–811, May 2006.
[39] V. Nikulshina, D. Hirsch, M. Mazzotti, and A. Steinfeld, “CO2 capture from air and co-production of H2 via the Ca(OH)2-CaCO3 cycle using concentrated solar power-Thermodynamic analysis,” *Energy*, vol. 31, no. 12, pp. 1379–1389, Sep. 2006.
[40] C. Tregambi, F. Montagnaro, P. Salatino, and R. Solimene, “Directly irradiated fluidized bed reactors for thermochemical processing and energy storage: Application to calcium looping,” in *AIP Conference Proceedings*, 2017, vol. 1850, no. 090007.

[41] C. Tregambi, P. Salatino, R. Solimene, and F. Montagnaro, “An experimental characterization of Calcium Looping integrated with concentrated solar power,” *Chem. Eng. J.*, vol. 331, pp. 794–802, Jan. 2018.

15. ANNEXES

15.1. Emissivity of a cloud of limestone in CO_2

This work is borne out of the VDI Heat Atlas, Part K [31].

15.1.1. Top-level calculation

The flux from the gas-particle mixture to the wall is calculated by

$$\dot{q}_{g+p,w} = \frac{\epsilon_w \sigma\left(\epsilon_{g+p} T_g^4 - \alpha_{g+p} T_w^4\right)}{\alpha_{g+p} + \epsilon_w - \alpha_{g+p}\epsilon_w}$$

The total emissivity of a gas-particle mixture ca be described as

$$\epsilon_{g+p} = (1-\beta)\left(\frac{1-\exp\left(-\Phi_{emi,g+p}\right)}{1+\beta\exp\left(-\Phi_{emi,g+p}\right)}\right)$$

Where

$$\gamma = \sqrt{1+\frac{2\bar{Q}_{bsc}}{\bar{Q}_{abs}}}$$

$$\beta = \frac{\gamma-1}{\gamma+1}$$

$$\Phi_{emi,g+p} = \left(\bar{Q}_{abs} A L_p + K_{emi,g}\right) l_{mb}\gamma$$

In a similar manner the absorptivity can be calculated:

$$\alpha_{g+p} = (1-\beta)\left(\frac{1-\exp\left(-\Phi_{abs,g+p}\right)}{1+\beta\exp\left(-\Phi_{abs,g+p}\right)}\right)$$

Where

$$\Phi_{abs,g+p} = \left(\bar{Q}_{abs} A L_p + K_{abs,g}\right) l_{mb}\gamma$$

L_p is the particle loading, in kg/m^3. The parameter l_{mb} is the mean beam length of radiation within the relevant geometry. A is the specific surface area of the particles.

15.1.2. Determination of particle absorption and scattering coefficients Q_{abs} and Q_{bsc}

This is performed graphically, and limestone is included on the graph in the Heat Atlas. The mean particle diameter d_p is measured experimentally, or can be calculated from the surface area and density of the particles by

$$d_p = \frac{3}{2\rho_p A}$$

15.1.3. Determination of gas absorption and scattering coefficients $K_{abs,g}$ and $K_{emi,g}$

These coefficients are defined as

$$K_{emi,g} = -\frac{\ln\left(1-\epsilon_g\right)}{l_{mb}}$$

$$K_{abs,g} = -\frac{\ln(1-A_v)}{l_{mb}}$$

Where ε_g is the emissivity of the gas and A_v is its absorptance. The value of ε_g varies with pressure, optical thickness and temperature. It is found using a graph in the Heat Atlas [31]. The absorptance A_v is a function of the wall and gas temperatures and the emissivity of the gas:

$$A_v = f_{p,CO_2}\left(\frac{T_g}{T_w}\right)^{0.65}\epsilon_g$$

The above is valid for CO_2. Note that $f_{p,CO2}$ is a pressure correction factor that at 1 bar total pressure is equal to 1.

15.2. Background to directly-irradiated calciners

This annex provides a brief overview of some directly-irradiated calciners and reactors mentioned in the existing literature. This list is not exhaustive.

15.2.1. The cyclone reactor- an atmospheric open solar reactor (Imhof, 1991) *[22]*

This paper describes, for the first time, the cyclone-type direct solar irradiator. It used the calcination of $CaCO_3$ as an example reaction. The reactor was a long conic right frustum (i.e. a cone with its point chopped off). A shallower, double-walled conic right frustum was placed in the top of the longer one, creating a cavity. The sunlight passed through the open top and bottom faces of the cone to reach the internal cavity. A stream of limestone and air was injected tangentially in to the cavity, which acted like a cyclone. The limestone calcined in the cyclone while being disengaged from the air and resulting CO_2; the solids passed out the bottom and the gases passed out between the two walls of the smaller frustum.

In the reference case, the particles were less than 10 μm in diameter and a baseline limestone:air mass ratio of 1:1 was used, equivalent to a molar ratio of 1:3.4, with 12 kg/h of each at typical conditions. The mean residence time was 0.5–1 second. The aperture was open to the atmosphere, although the author stated that there was little leakage into the reactor. The radiant energy flux was 18–28 kW, with a maximum radiant flux density of 3–6 MW/m^2 depending on the time of day and season. This reactor was then investigated in another paper [32].

15.2.2. Some physical and chemical experiments under concentrated solar radiation and some thermodynamic considerations (Durisch, 1991) *[33]*

This paper acted as a discussion and presentation of various tests performed at the Paul Scherrer Institute (PSI) in Switzerland as a precursor to more high-temperature trials. The tests were not within any particular reactor or environment apart from air. It presents an interesting but incorrect theory about the effective temperature of irradiated surfaces, based on the chemical potential of radiation. However, non-zero chemical potential of radiation exists only for non-thermal radiation (i.e. radiation whose spectrum is not dependent upon the temperature of the emitter); since sunlight is thermal radiation its chemical potential is zero.

15.2.3. Experimental Investigation of an Atmospheric-Open Cyclone Solar Reactor for Solid-Gas Thermochemical Reactions (Steinfeld, Imhof & Mischler 1992) *[32]*

This paper uses a smaller version of the reactor designed and built in a previous paper [22] to investigate the effectiveness of solar radiation for limestone calcination. It has a peak flux concentration of 6 MW/m^2. The reactor is 30 cm high with a 10° angle on the main cone; the aperture between the larger and smaller cones is 6 cm. The walls were insulated with inorganic wool. Unlike the previous design, the reactor was placed horizontally, i.e. with the faces of the top and bottom of the cone being vertical instead of horizontal.

The smaller, upper conic right frustum was a water cooled double wall as it comes into contact with direct solar radiation. The apparent absorptance of the reactor is 0.97 despite the walls' absorptance of 0.36.

$CaCO_3$ was fed along with compressed air tangentially into the cylindrical part of the large cone. The calcined product falls out of the 'bottom' of the cone and the CO_2 leaves near the top of the reactor (i.e. it is counter-current). Suction applied at the gas outlet prevented dust release.

The loading ratio, defined as the ratio of solid to gas mass flow through the inlet, was around 0.1. The powder was 1–5 µm $CaCO_3$. 0.6 kg/h $CaCO_3$ and 6 kg/h air were fed at 298 K; the gas outlet exited at 820 K but was probably diluted by air entering through the aperture. Around 43% of the energy entering the aperture was transferred to the materials and gases, but there are errors around this due to the false air. The aperture only received 41% of the energy directed by the mirrors and heliostat, so the total efficiency drops to 18%.

Calcination extents of 53–94% were obtained, although handling of the calcined materials was not particularly careful and so many of the samples had partially hydrated; it can be expected that a small amount of recarbonation also occurred.

15.2.4. Decomposition of limestone in a solar reactor *[34]* (Imhof 1996)

This Paul Scherrer Institute paper investigated the degree of calcination of limestone, both in pure form and as part of cement raw meal. A scaled-up version of the previous cyclone reactor was developed, with a nominal power of 60 kW. Natural white limestone reached a calcination of 38–54%, whereas dark limestone reached 52–58%. Two cement raw meals were tested, the HCB version calcining 52–72% and the PSI one 32–85%.

15.2.5. A Solar Chemical Reactor For Co-Production Of Zinc And Synthesis Gas (Steinfeld et al. 1998) *[35]*

This paper came from the same Paul Scherrer Institute group as [22], [32]. The reactor's conical axis was placed horizontally, and the material tangentially injected at the tip end of the conic frustum rather than the base as was the case in the limestone versions. As it involved the generation of Zn and syngas from ZnO and CH_4, it had to be gas-tight and a window was installed in the aperture. This was kept free of particles by a flow of gas injected across the window's surface. The reactants' temperature was raised from 800 to 1200–1600 K. The scientists found that Zn vapour would condense on the window when the fresh methane flow across the window to protect it was low. This suggests that this is a necessary component of the system.

15.2.6. Design and experimental investigation of a horizontal rotary reactor for the solar thermal production of lime (Meier et al, 2004) *[36]*

This paper from the Paul Scherrer group looks at a rotary kiln for deadburned lime manufacture. A lab-scale (15 kW, 3000 sun) reactor was designed and built. The kiln was conical in shape, allowing perfectly horizontal installation and also better solar penetration to the front end of the kiln.

Extents of calcination of 1–5 mm limestone particles reached up to 98%, and the reactivity of the product varied significantly, with a t_{60} range of 14 s – 38 min. Approximately 20% of the solar energy went into the calcination reaction.

15.2.7. Multitube Rotary Kiln for the Industrial Solar Production of Lime (Meier et al, 2005) *[37]*

In this paper, the rotary kiln concept tested in the previous year's paper was adapted so that there were many tubes surrounding a central receiver cavity. The cavity was made of SiC. The kiln/receiver was slightly tilted off horizontal, so that material moved through the tubes. At the back of the receiver was a preheating area which also acted to regulate solid passage into the tubes.

The unit was built to the same size as the other kiln (15 kW, 3000 sun concentration, 8 cm aperture) and used the same limestone particle size (1–5 mm). The residence time was 5–8 minutes. Greater than 95% calcination was achieved at temperatures 1200–1400 K. The authors believed scale-up to 100–1000 kW would be relatively simple.

15.2.8. Hydrogen production by steam-gasification of petroleum coke using concentrated solar power—II Reactor design, testing, and modelling (Z'Graggen et al., 2006) *[38]*

This paper uses a 6.6 MW horizontal axis solar furnace operating at 1300–1800 K, with a residence time for the material of approximately 1 second. The reactor was atmospherically sealed, that is, it incorporated a quartz window. A solar-to-chemical efficiency of 9% was achieved, rising to 20% once heat integration was included. Petcoke and steam single-pass conversions were up to 87% and 69%, and the quality of the syngas was higher than using traditional internal combustion methods.

15.2.9. CO2 capture from air and co-production of H2 via the Ca(OH)2–CaCO3 cycle using concentrated solar power – Thermodynamic analysis (Nikulshina et al. 2006) *[39]*

This paper focusses on the capture of CO_2 from the air using $Ca(OH)_2$ generated by slaking CaO created by solar calcining $CaCO_3$ from the capture step. The $Ca(OH)_2$ was in solution and a typical scrubbing unit was used to capture to CO_2. Further, there was an option to generate CO-rich syngas in the process by injecting CH_4 into the solar calciner. Here,

$$CaCO_3 + CH_4 \leftrightarrow CaO + 2H_2 + 2\,CO$$

This process is highly endothermic and thermodynamically attractive only above 1300 K, meaning that very high temperatures were required in the solar calciner. The energy requirement without heat integration is 12.4 MJ/mol CO_2 captured (co-generation of 4 mol H_2); with heat integration (many solid-gas heat exchangers) it falls to 2.8 MJ/mol CO_2, or 64 GJ/t CO_2 captured. Only 22 GJ_{LHV} H_2 is generated per tonne CO_2 captured, giving a net energy intensity of 42 GJ/t CO_2.

15.2.10. Directly irradiated fluidized bed reactors for thermochemical processing and energy storage: Application to calcium looping (Tregambi et al. 2017) *[40]*

In this paper, a bubbling fluidised bed of sand and limestone was irradiated with simulated sunlight to effect calcination. Its height and diameter were both 0.1 m. Total flux is 3.2 kW, with a maximum concentration of 3000 kW/m^2. Two electrical heaters were used to control the temperature when the radiation was not in use, i.e. during carbonation and between carbonation and calcination conditions.

In the first test, only silica sand (420–590 µm) was used. The top layer of the bed was irradiated, which meant that average temperatures of around 1000 °C were seen, with centre point temperatures rising to 1000–1100 °C and hot spots around 1000–1200 °C. A thermocouple 1 cm below the bed surface measured temperatures around 950 °C and one further in the bed saw 925 °C.

In the second tests, 120 g of limestone (420–590 µm) and 730 g silica sand (850–1000 µm) was used, with the former being injected only once the reactor was at the correct condition. The bed surface only reached around 950 °C, and the thermocouples reached approximately 910 and 890 °C, respectively. Hot spots did not exceed 1100 °C and the centre of the surface rarely exceeded 1000 °C.

In the second case, a deviation from the expected temperature trajectories is seen in the 250–450 s time range. This can be attributed to calcination; the lower steady state temperatures in the second test compared with the first are probably due to the lower absorptivity of limestone than silica sand.

In both tests, the standard deviation of the temperature measurements at the thermocouples in the bed was around 10–20% that on the surface and at hot spots. This may be due to differences in measurement technique, as the surface was measured using an IR camera and the

bed temperature by Type K thermocouples. Alternatively, the temperature of the bed surface may vary more than deeper in the bed where there is better non-radiative heat transfer.

15.2.11. An experimental characterization of Calcium Looping integrated with concentrated solar power (Tregambi et al. 2018) *[41]*

This journal paper builds upon the conference paper published in 2017. More detail is provided. For example, a plot of CO_2 release over the course of a calcination half-cycle is given. Most CO_2 is released before the temperatures reach their maxima; this makes estimating kinetics more difficult. Furthermore, the large particle size leads to heat and mass transport limitations that will be less severe in powders.

This paper also found that sintering appears to be a bigger issue in solar calcination than normal calcination; a 30% smaller cumulative pore volume between 0.1 & 50 nm was identified, and the BET surface area was 20% smaller after three calcinations. No substantial particle size distribution differences were found between the solar heated and conventionally heated particles.

Particle over-temperatures of 45 °C were found across the surface of the bed, rising to 80 °C within hot spots.